



CONCORDIA UNIVERSITY  
PHYSICS DEPARTMENT

---

# Improved back end electronics enclosure for the ALBATROS interferometer on Marion island

---

*Author:*  
Mariya Krasteva

*Supervisors:*  
Prof. Cynthia Chiang  
Prof. Matt Dobbs

A thesis submitted for the degree of  
*BSc Honours Physics*

May 1, 2019

## Abstract

The Probing Radio Intensity at High-Z from Marion (PRIZM) experiment is situated on the Marion island midway between South Africa and Antarctica. The experiment is looking into the epoch of the cosmic dawn: when luminous objects first formed. The radio telescopes in place will measure the redshifted 21-cm hydrogen line at low frequencies with the first telescope centered at 70 MHz and the second centered at 100 MHz aiming to confirm the recent result from the EDGES experiment. A complementary project to PRIZM will be the Array of Long Baseline Antennas for Taking Radio Observations from the Sub-antarctic (ALBATROS) which will be mapping the sky by using an array of autonomous antennas down to frequencies of a few MHz.

The main focus of this thesis is the improved design for the back end electronics enclosure for the ALBATROS project. More precisely, the design of the SNAP box will be optimized for RF tightness between electronic components. The goal will be to better understand the behavior of the instrument at frequencies down to  $<10$  MHz which should coincide with the dark ages, an epoch at even higher redshifts than the cosmic dawn. Given that Marion island is one of the most radio quiet places on Earth combined with the upcoming solar minimum expected in spring 2019, the PRIZM and ALBATROS experiments will have favorable observing conditions to probe the relatively unexplored low frequencies. These two projects aim to constrain the theoretical predictions through observations of the redshifted sky-averaged 21-cm brightness as a function of frequency. Such models predict the evolution of the universe's average temperature and the physical implications behind these fluctuations.

The frequency range investigated by these two experiments corresponds to the epoch of the dark ages and the cosmic dawn. These frequencies are challenging for ground based observations because of the man-made radio frequency interference (RFI) and the brightness of our milky way. With a good understanding of the instrument and with the most radio quiet observing location, the ALBATROS team is hoping to improve the sky mapping at these frequencies, which has last been mapped in the late 60's and 70's.

## Acknowledgements

I would like to thank my supervisor Professor Cynthia Chiang for being so patient, for her kindness and for her contagious enthusiasm about cosmology.

I would like to thank Professor Matt Dobbs for his support and for introducing me to the world of interferometry back when I was a first year undergraduate.

I want to acknowledge the support and understanding of Professor Alexandre Champagne who believed in me despite my unusual academic path. Thanks to Professor Laszlo Kalman for his advice and words of encouragement. I would also like to acknowledge Professor Mariana Frank, Christophe Grova, and Pablo Bianucci for sharing their love for physics and being an inspiration throughout my bachelor degree.

Finally, I am infinitely grateful towards my classmates for making every derivation a shared struggle, and most importantly I would like to thank my family and Sergio for their incredible support throughout the years.

# Contents

<b>1</b>	<b>Introduction</b>	<b>5</b>
1.1	The Field of Cosmology . . . . .	5
1.2	21-cm Cosmology . . . . .	7
1.3	Interferometry . . . . .	8
1.3.1	Low frequencies experiments . . . . .	10
1.3.2	EMI, RFI, Galactic Noise, and Ionosphere . . . . .	12
<b>2</b>	<b>Background</b>	<b>16</b>
2.1	The PRI <sup>Z</sup> M experiment . . . . .	16
2.2	ALBATROS-EGG experiment and ALBATROS Interferometer . . . . .	17
2.3	ALBATROS Instrumentation . . . . .	19
2.3.1	LWA antenna . . . . .	20
2.3.2	Active Balun . . . . .	21
2.4	ALBATROS Signal Processing . . . . .	21
2.4.1	Signal Processing . . . . .	22
2.4.2	Back end electronics . . . . .	23
<b>3</b>	<b>Enclosure Design</b>	<b>26</b>
3.1	Previous Enclosures . . . . .	26
3.2	Improved Design . . . . .	28
3.3	Components Layout . . . . .	30
3.3.1	Enclosure Shielding Effectiveness . . . . .	32
3.4	Gasket Considerations . . . . .	38
3.5	SolidWorks Software . . . . .	40
<b>4</b>	<b>Conclusions</b>	<b>43</b>
	<b>Bibliography</b>	<b>46</b>

# List of Figures

1.1	This schematic of the history of the universe illustrates where the dark ages stand with respect to afterglow (CMB) and the first stars [1]. . . . .	7
1.2	Hyperfine splitting of neutral hydrogen: parallel spins and antiparallel spins [2] . . . . .	8
1.3	A single dish telescope sliced in many segments with their signals added is the first step towards the equivalent of a radio interferometer [3] . . . . .	9
1.4	If the segments are placed on the ground, their signals need to be combined and the time delays accounted for to create a radio interferometer [3]. . . . .	9
1.5	Low frequency 21-cm tomography experiments at redshift $5 < z < 27$ [4]. 1. The Owens Valley Long Wavelength Array (OVRO-LWA) 2. Low Frequency Array (LOFAR) 3. Giant Metrewave Radio Telescope (GMRT) 4. Murchison Widefield Array (MWA) 5. Hydrogen Epoch of Reionization Array (HERA) . . . . .	11
1.6	Low frequency 21-cm global signal experiments [4]. 1. Experiment to Detect the Global EoR Signature (EDGES) 2. Probing Radio Intensity at high-Z from Marion (PRI <sup>z</sup> M) 3. Large Aperture Experiment to Detect the Dark Ages (LEDA) 4. Cosmic Twilight Polarimeter (CTP) 5. SARAS 2. . . . .	12
1.7	RFI characterization on Marion island's main base and PRI <sup>z</sup> M site (same for ALBATROS) [5]. At the main base signals from boat transponders and helicopter communications are present. The PRI <sup>z</sup> M site on the other hand has almost no RFI. . . . .	14
1.8	Ionosphere activity predictions from 2007 in the southern hemisphere [5]. . . . .	15
1.9	Galactic foreground mapped at 408 MHz [6]. . . . .	15
2.1	Sky brightness of the 21-cm signal as a function of redshift and observation frequency [7]: a) 21-cm tomography measuring the temperature brightness variations, b) global signal temperature brightness variations and the respective events they represent. . . . .	17
2.2	Experimental setup of the PRIZM and ALBATROS-EGG experiment on Marion island [8] . . . . .	18
2.3	State of the art mapping at 2.1 MHz [9] . . . . .	19

2.4	The projected distribution for the ALBATROS interferometer will correspond to the current hut distribution on Marion island [8]. . . . .	20
2.5	The LWA antenna on Marion island with the two dipoles shaped like a bow-tie hanging above the wire mesh layed on the ground [8]	21
2.6	Active balun as located on the LWA antenna and a schematic illustrating the inner workings of the active balun [8] . . . . .	22
2.7	ALBATROS-EGG simplfied schematic for the back end electronics [8] . . . . .	23
2.8	ALBATROS back end electronics wiring diagram. This schematic shows the new components with respect to the previous ALBATROS-EGG experiment. . . . .	24
2.9	This figure illustrates the main features of the SNAP board. For the purpose of this experiment only two ADC analog inputs, one clock/PPS input, and the Raspberry Pi interface will be used. [10]	25
3.1	ALBATROS-EGG SNAP Enclosure showing gaps at the corners and signal processing chains containing the amplifiers within the same space as the SNAP board. . . . .	27
3.2	Improved ALBATROS-EGG enclosure design with four inputs and shielded connectors. . . . .	27
3.3	New ALBATROS enclosure design: (a) power input, (b) LWA antennas input, (c) GPS receiver input, and (d) Ethernet input. . . . .	28
3.4	Bottom-back view of the ALBATROS enclosure showing the SNAP board location (a) and the RF clean space (b). . . . .	29
3.5	Bottom view of lower half of the ALBATROS enclosure showing the location of the Raspberry Pi connection in the bottom-right corner. . . . .	30
3.6	Exploded view of the ALBATROS new enclosure . . . . .	31
3.7	Component layout and the corresponding photo montage of the bottom part of the shelf and top part of the shelf respectively (not to scale) assuming the top of the picture is the front panel where all the inputs are. The axis of symmetry is along the y-axis between the two pictures. . . . .	32
3.8	Shielding effectiveness of a 2mm aluminum sheet with the source located at 1 cm away. . . . .	34
3.9	Plane wave shielding effectiveness of a 2 mm aluminum sheet with the source located at 10 m away. . . . .	35
3.10	Shielding effectiveness of a 0.01 mm aluminum sheet with the source located at 1 cm away. . . . .	36
3.11	Shielding effectiveness considering holes without screws and edge gaps of 2mm. . . . .	37
3.12	Shielding effectiveness for the entire enclosure considering holes without screws and edge gaps of 2mm. . . . .	38
3.13	Finger stock beryllium copper gasket [11] . . . . .	39
3.14	SolidWorks assembly screen capture . . . . .	41

# Chapter 1

## Introduction

Every field of physics is trying to peer deeper into the nature of things that surround us, influence us, and compose the world around us. This need to answer the question "why" is what makes us all human, and perhaps, all physicists in a way. Cosmology is the field of astrophysics trying to determine how it all started and how it is evolving. However answering a simple question often generates even more questions which in turn generates even more questions and research projects.

In this work, a brief history of the field will be presented followed by a description of 21-cm cosmology and how interferometry is used in experimental cosmology. An emphasis will be made on the ALBATROS experiment which aims to observe the sky at frequencies for which the data is very scarce. This interferometer currently under development will be deployed on Marion island, a volcanic island situated midway between Antarctica and South Africa. For the hardware to survive in these harsh conditions it needs to be small and autonomous. After some lessons learned from the PRI<sup>Z</sup>M experiment and the ALBATROS-EGG experiment, the hardware needs to be upgraded before it is replicated into many small autonomous observing stations. The main object of this thesis is an improved design for the back end electronics enclosure. This design was developed to be flexible for future modifications and possible use for the McGill Arctic Research Station.

### 1.1 The Field of Cosmology

What happened after the Big Bang? The entire 13.7 billion years of history of the universe are safely preserved into the sky thanks to the finite speed of light. To go back in time astronomers simply travel across the electromagnetic spectrum to observe a given feature at different frequencies. Since the universe is expanding, the original signal gets redshifted, meaning that the oldest emitted light will have its wavelength more stretched than light coming from the same phenomenon at a more recent time. This effect can also be experienced through the Doppler shift

of sound waves. The redshift  $z$  is defined in 1.1 where  $\beta = \frac{v}{c}$ :

$$z = \frac{\lambda_{obs} - \lambda_{rest}}{\lambda_{rest}} = \sqrt{\frac{1 + \beta}{1 - \beta}} - 1 \quad (1.1)$$

The field of cosmology studies the origins of the universe and its evolution. The first glow, 380 000 years after the Big Bang, is the Cosmic Microwave Background (CMB) which was accidentally discovered in 1964 by Radio Astronomers Robert Wilson and Arno Penzias [12]. This discovery motivated decades of experimental cosmology until the present days. Many space telescopes as well as ground telescopes have been built to study the early universe. Some good examples are the Hubble Space Telescope (HST), NASA's Cosmic Background Explorer (COBE), the Keck, Subaru, and VLT.

From the Big Bang until  $10^{-34}$  s after it occurred is the Planck epoch: a state of the universe during which only energy existed and all forces were combined into one superforce. The current understanding of the physics after the Big Bang starts at  $10^{-34}$  s when gravity divided from the other forces and became distinguishable [13]. From  $10^{-34}$  s until  $10^{-35}$  s was the Grand Unified Theory (GUT) epoch. What followed was inflation, an epoch during which the universe expanded and cooled enough so that the strong nuclear force became distinguishable from the remaining electroweak force. During the remaining epochs of the radiation dominated era all four fundamental forces became distinguishable, sub-atomic particles formed and helium was first formed.

At  $z \approx 1100$  is when matter and radiation decoupled and hydrogen atoms started forming during what is referred as the recombination period [13]. This radiation decoupling occurred 380 000 years after the Big Bang and formed the Cosmic Microwave Background (CMB). The Dark Ages is the period between the first released photons from the CMB and the first stars. It is precisely during the Dark Ages that the first hydrogen atoms formed, but until stars were formed, no photons were released beyond the ones coming from the CMB. Figure 1.2 shows a schematic of the timeline described above.

While there are a lot of observations of the CMB and distant Galaxies, the epoch of the Dark Ages ( $1100 > z > 30$ ), the Cosmic Dawn and reionization ( $30 > z > 6$ ) are relatively unexplored [7]. The theoretical predictions for this time period are yet to be verified by observation.

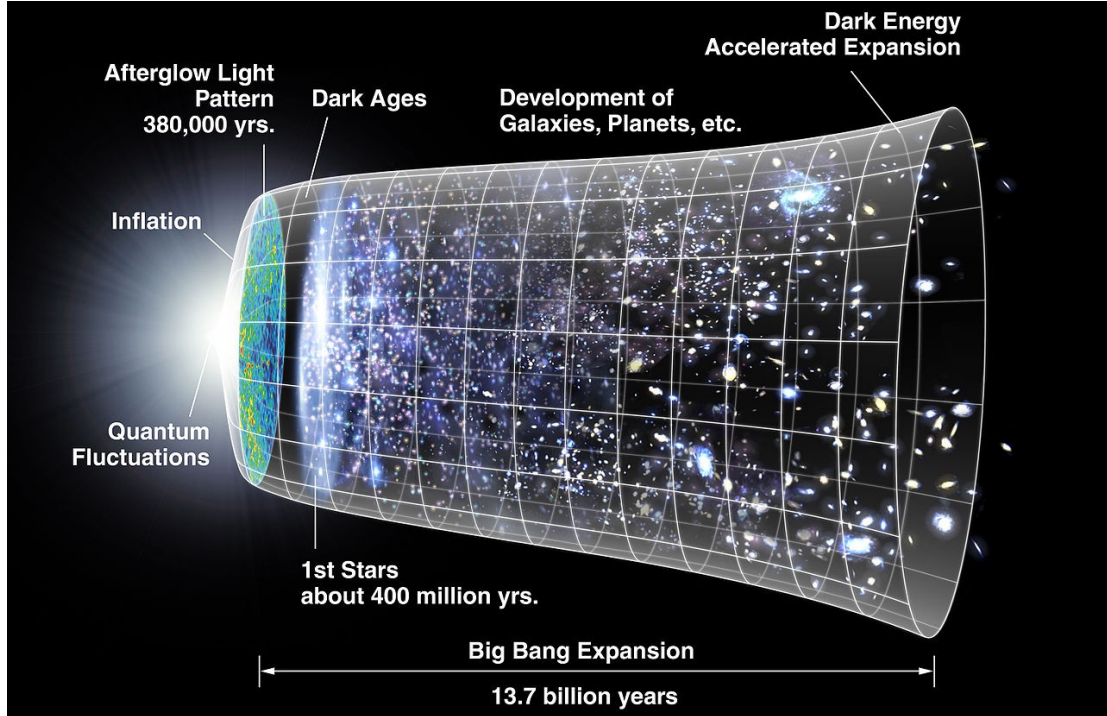


Figure 1.1: This schematic of the history of the universe illustrates where the dark ages stand with respect to afterglow (CMB) and the first stars [1].

## 1.2 21-cm Cosmology

The early universe contained primarily hydrogen, which later on fuelled stars. The signature of the presence of hydrogen is the 21-cm emission line. To understand its distribution and abundance, astronomers need to map the whole sky, and to understand hydrogen's time evolution they need to do this mapping at different redshifts to observe different epochs of the universe.

The 21-cm emission line arises from the hyperfine splitting of the hydrogen atom. Neutral hydrogen is one proton and one electron. In the ground state of neutral hydrogen, the wave function is spherically symmetric. Solving for the energy it is found that it depends on the dot product between the electron spin and the proton spin, called spin-spin coupling [14]:

$$E_{hf} = \frac{\mu_0 g_p e^2}{3\pi m_p m_e a^3} \langle \mathbf{S}_p \cdot \mathbf{S}_e \rangle \quad (1.2)$$

Working out the dot product, we find that there are two possible states. Either the two spins are parallel which result in a higher energy, or the two spins are antiparallel resulting in a lower energy.

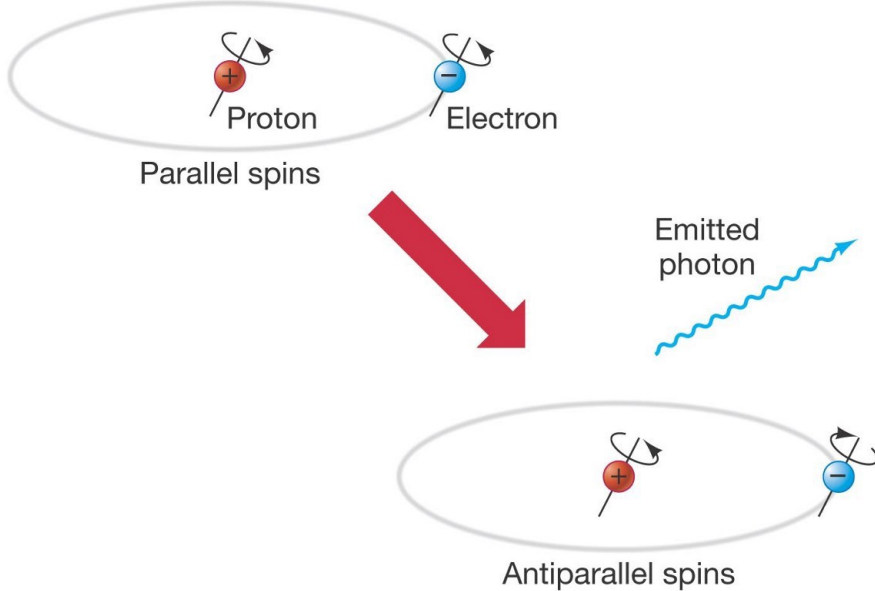


Figure 1.2: Hyperfine splitting of neutral hydrogen: parallel spins and antiparallel spins [2]

The resulting energy difference from the spin flip of the electron emits a photon with a frequency of 1420 MHz which corresponds to the 21 cm emission line, one of the most precisely known quantities in astronomy. In fact, this signal can reveal much more than simply acknowledging the presence of hydrogen. Spin temperature fluctuations, the mass of neutrinos, and the initial conditions during the early universe can also be derived from this signal by looking at the power spectrum [7].

This 21 cm signal from hydrogen is redshifted because of the expansion of the universe. The higher the redshift, the earlier in the history of the universe the signal is originating. The 21 cm signals with the highest redshift come from the Dark Ages, when the first hydrogen atoms started forming from the inhomogeneities in the CMB, but still no stars existed [7]. The more structures kept appearing, the more the 21 cm signal fluctuated in density over time.

### 1.3 Interferometry

To characterize the evolution of hydrogen, several experiments have been put into place to map the hydrogen distribution at different times and verify our theoretical understanding of fundamental physics. However, characterizing density changes across the sky calls for telescopes with a high resolution and high sensitivity which in turn translates to large collecting areas. The redshifted 21 cm signal is in the radio part of the light spectrum. Given the long radio waves, a good resolution

is even more difficult to obtain. In addition to these constraints, the Earth's atmosphere is not transparent to all light and galactic noise also poses a problem at these frequencies [15].

There are several ways to meet the desired requirements for sensitivity and resolution. In terms of radio telescopes the problem can be summarized to either a single dish or a collection of small dishes forming an interferometer. Figure 1.3 and 1.4 show how the later is actually equivalent to a single dish.

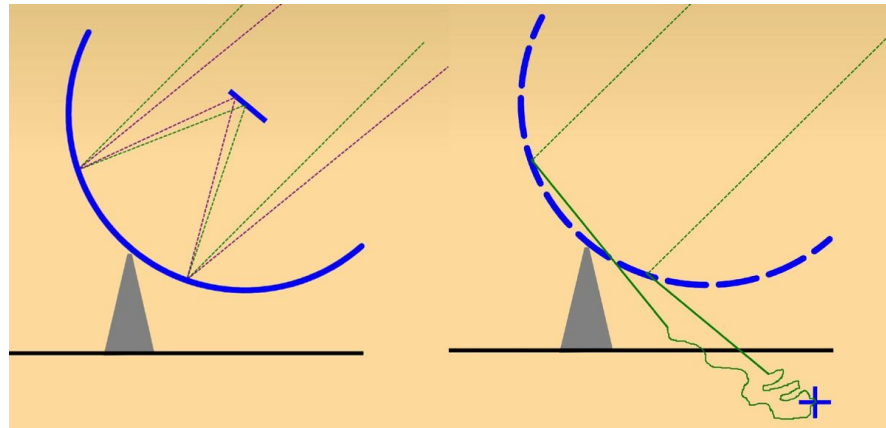


Figure 1.3: A single dish telescope sliced in many segments with their signals added is the first step towards the equivalent of a radio interferometer [3]

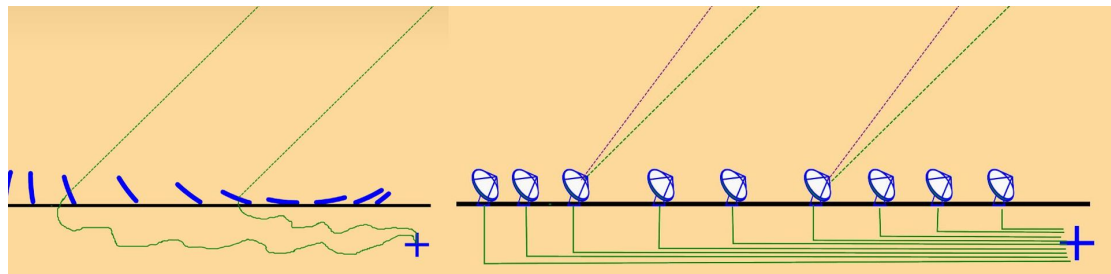


Figure 1.4: If the segments are placed on the ground, their signals need to be combined and the time delays accounted for to create a radio interferometer [3].

Interferometry uses a similar idea as the double-slit experiment. An interference pattern is measured with a resolution proportional to  $\lambda/B$ , where  $B$  is the longest baseline between two receivers [3]. Therefore, to achieve the best resolution for the overall array, the baseline needs to be as large as possible.

Once the array of telescopes has been created and the time delays have been accounted for, the signals need to be synthesized such that the light is all "focused

at one point". In a regular single dish telescope, all beams will be redirected towards the receiver at the focus of the telescope in order to see an image. However, in an interferometer this needs to be achieved using a Fourier transform to go from the  $uv$ -plane which is the distribution of the receivers in space to the image plane which is the 2D imaged obtained [3]:

$$T(x, y) = \int \int V(u, v) e^{2\pi i(ux+vy)} dudv \quad (1.3)$$

To see very faint signals, the sensitivity  $\sigma_S$  needs to be increased. This can be done by decreasing the temperature of the system which decreases the overall noise in the instrument. It can also be done by increasing the collecting area ( $A_{eff}$ ), increasing the bandwidth  $\Delta\nu$  or increasing the observation time  $\tau$  by taking long exposures [3].

$$\sigma_S = \frac{T_{sys}}{A_{eff}\sqrt{\Delta\nu \cdot \tau}} \quad (1.4)$$

For frequencies higher than 500MHz single dish telescopes are the optimal solution since synthesizing and calibrating for high frequency signals is much more difficult than low frequency signals in additions of the electronics being much more expensive. However, for lower frequencies, these restrictions do not apply. Therefore, many small and cost effective receivers can be put in place without any moving parts.

There are a few limiting factors to telescope arrays. The maximum baseline  $D_{max}$  and the minimum baseline  $D_{min}$  set the limits on the angular resolution:  $\lambda/D_{max} - \lambda/D_{min}$  [16]. Additionally, the field of view of a single telescope  $\lambda/d$ , where  $d$  is the diameter of the aperture as well as the number of telescopes set a limit on the field of view of the telescope and thus the kind of sources that can be seen [16].

### 1.3.1 Low frequencies experiments

Several ground-based experiments are currently observing at low frequencies to study the 21-cm signal from the early universe. These experiments are categorized as 21-cm tomography, and global 21 cm signal experiments.

#### **21-cm Tomography:**

These experiments investigate the temperature brightness fluctuations of the 21-cm signal. The main results are in the form of 3D heat maps revealing information about the variations of neutral hydrogen and spin temperature [17].

The resolution required to chart these small changes in the signal needs to be as high as possible. This requirement is usually met with large radio interferometers. Table 1.1 and Figure 1.5 show a few examples of such arrays.

Experiment	Redshift $z$	Frequency Range (MHz)	Location
GMRT	$z < 8.5$	150 – 1500	Khodad
MWA	$4 < z < 19$	70 – 300	Murchison
HERA	$5 < z < 27$	50 – 250	Karoo
OVRO-LWA	$16 < z < 50$	27 – 85	Owens Valley
LOFAR	$5 < z < 50$	30 – 240	Netherlands

Table 1.1: Fluctuations of the 21-cm signal experiments at redshift  $5 < z < 27$  [4]

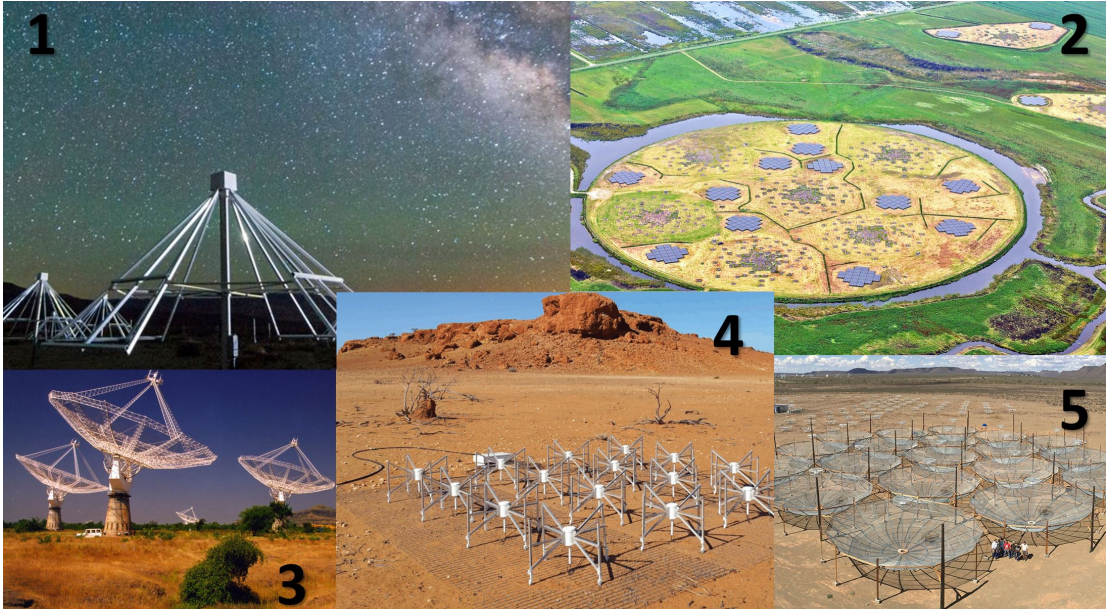


Figure 1.5: Low frequency 21-cm tomography experiments at redshift  $5 < z < 27$  [4]. 1. The Owens Valley Long Wavelength Array (OVRO-LWA) 2. Low Frequency Array (LOFAR) 3. Giant Metrewave Radio Telescope (GMRT) 4. Murchison Widefield Array (MWA) 5. Hydrogen Epoch of Reionization Array (HERA)

### Global Signal Experiments:

Measuring the brightness temperature of the global 21-cm signal as a function of frequency reveals information about the evolution of the signal through time. The global signal variation constrains the different epochs and physical processes occurring at a given time in the history of the early universe as shown in more detail in Figure 2.1. To measure this signal few antennas are necessary, but careful calibration and noise removal techniques are necessary to track the signal temperature brightness variations.

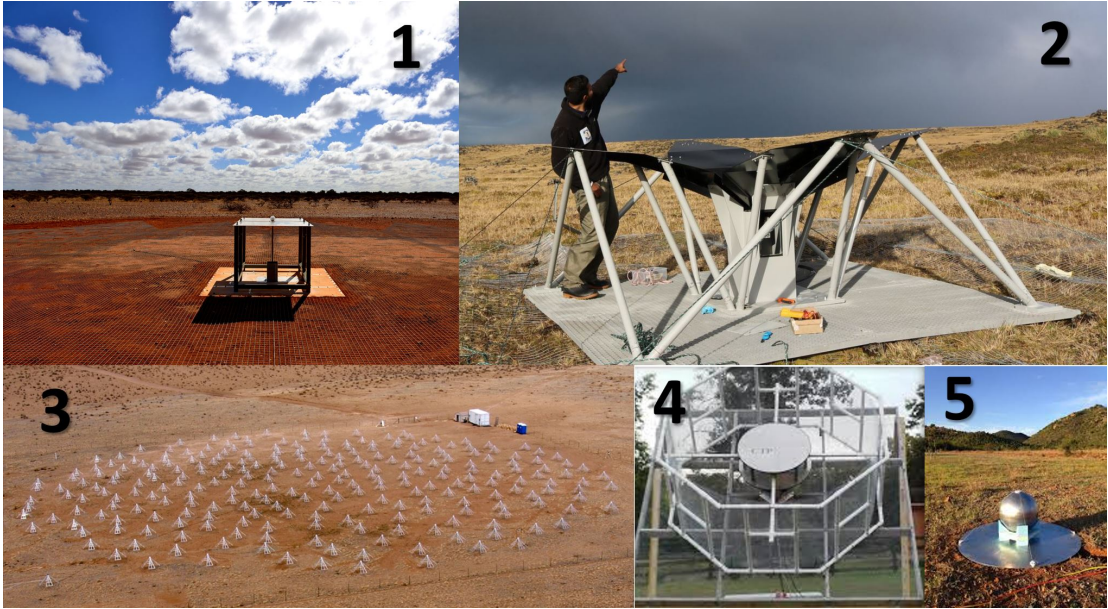


Figure 1.6: Low frequency 21-cm global signal experiments [4]. 1. Experiment to Detect the Global EoR Signature (EDGES) 2. Probing Radio Intensity at high-Z from Marion (PRI<sup>z</sup>M) 3. Large Aperture Experiment to Detect the Dark Ages (LEDA) 4. Cosmic Twilight Polarimeter (CTP) 5. SARAS 2.

Experiment	Redshift $z$	Frequency Range (MHz)	Location
EDGES	$6.5 < z < 28$	50 – 200 MHz	Murchison Radio Obs.
PRI <sup>z</sup> M	$13 < z < 19$	30 – 200 MHz	Marion Island
LEDA	$15 < z < 30$	30 – 88 MHz	Owens Valley
SARAS2	$6 < z < 30$	87.5 – 175 MHz	Gauribidanur Obs., India
CTP		60 – 120 MHz	Green Bank

Table 1.2: Global 21-cm signal experiments [4]

### 1.3.2 EMI, RFI, Galactic Noise, and Ionosphere

Observing faint signals from the early universe comes with many technical challenges. Some of them are caused by instrumental or man-made interference while other louder signals are from natural origins. Understanding these loud signals and the atmospheric effects when observing from ground are key to the design and calibration of the instruments as well as to the data analysis.

#### Electromagnetic Interference (EMI):

Electromagnetic Interference (EMI) is typically caused by operating electronics which generate an electromagnetic field around them. The interference be-

tween the fields of the electrical components can induce an unwanted signal at the receiver or in the readout electronics. In the context of radio telescopes this is particularly important since any wire can act as an antenna and the observing frequencies are often in a similar range as the EMI produced by the signal processing electronics.

To separate the signal from the EMI noise, enclosures acting as Faraday cages are built around the components generating the most EMI. Shielding effectiveness is what quantifies the attenuation of EMI within the system. Shielding is most effective when it is done directly at the source. Enclosures made of conducting materials such as copper or aluminum are very effective at reducing EMI. The effectiveness also depends on the thickness of the material used and the apertures present in the enclosure (more details in section 3.3.1).

### **Radio Frequency Interference (RFI):**

Radio Frequency Interference (RFI) is typically caused by man-made radio signals such as radio stations, satellite signals, Wi-Fi signals, or even microwaves ovens. As city lights outshine the sky making optical astronomy nearly impossible at these locations, the same goes for RFI and radio astronomy. To observe faint cosmological signals, astronomers need to build telescopes in very remote places. Even very far way, telescopes are optimized to detect extremely faint signals, which makes it possible to pick up RFI that has originated kilometers away.

The ALBATROS project is no exception. Marion island was specifically chosen for being very radio quiet and far away from civilization. At frequencies below 200 MHz, the observation band is mostly dominated by FM radios. Fortunately, the RFI on Marion island is very low, and no FM radio bands were recorded. Figure 1.7 shows results from the RFI characterization done on Marion island in 2017.

### **Ionosphere:**

The ionosphere is a layer of atmosphere composed of ionized plasma located 75-1000 km above Earth's surface. The Sun's UV and X-ray light is the primary cause of ionization of this layer [18]. During periods of high solar activity, the ionosphere becomes almost opaque at low frequencies allowing ham radio amateurs to use it to bounce low frequency waves and communicate signals to another continent altogether. This phenomenon is of course very problematic for cosmological observations at low frequencies increasing the risks of RFI even in remote locations. The solar activity is therefore a limiting factor during observations. The best times to observe are therefore during a solar minimum or at night when the ionosphere is only ionized by cosmic rays. However, an ionosphere study for the LOFAR experiment reported that the data is also affected by ionosphere scintillation events during night causing loss of data [18]. Therefore, the ionosphere conditions above the experiment site must be very carefully monitored. Figure 1.8 shows the ionosphere activity above Marion island.

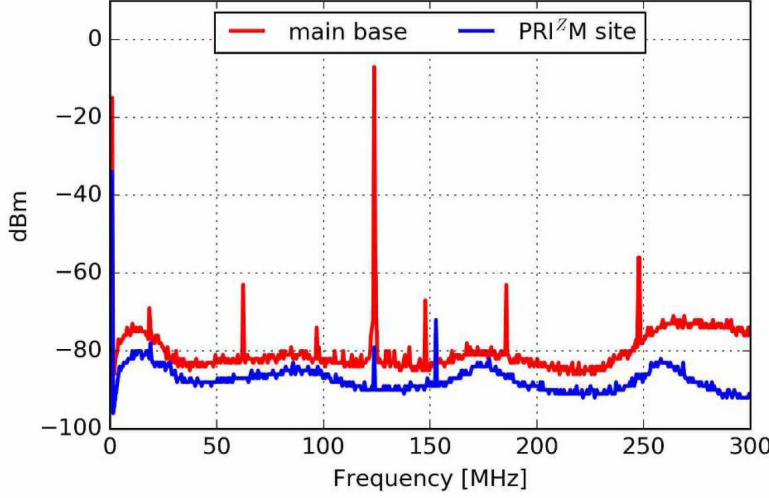


Figure 1.7: RFI characterization on Marion island’s main base and PRI<sup>z</sup>M site (same for ALBATROS) [5]. At the main base signals from boat transponders and helicopter communications are present. The PRI<sup>z</sup>M site on the other hand has almost no RFI.

#### Galactic Noise:

At frequencies below 300 MHz, there is an additional source of RFI which is the noise generated from galactic synchrotron radiation. The radiation is caused by relativistic electrons being accelerated by the magnetic field within the galaxy [19]. Figure 1.9 shows the galactic foreground noise produced at 408 MHz. According to results shown at the radio synchrotron background workshop (2017), the sky temperature follows a power-law rise at frequencies below  $\sim 10$  GHz [19]. Therefore, the galactic noise is expected to be one of the dominant signals recorded at very low frequencies.

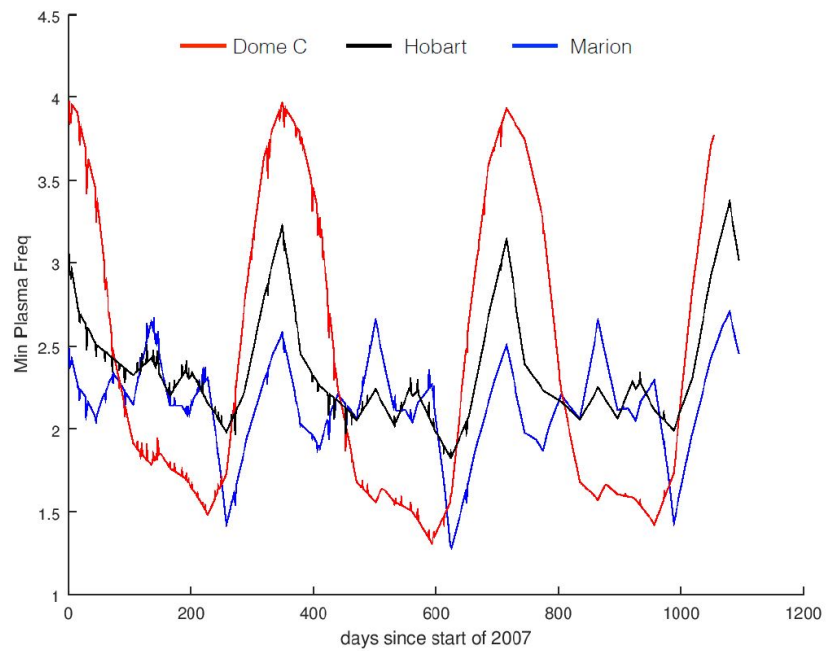


Figure 1.8: Ionosphere activity predictions from 2007 in the southern hemisphere [5].

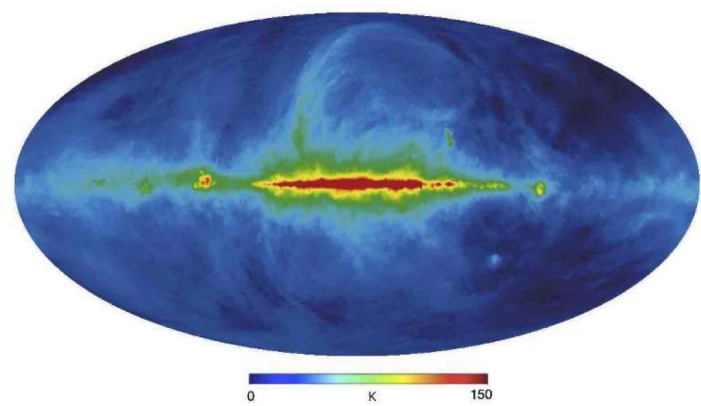


Figure 1.9: Galactic foreground mapped at 408 MHz [6].

# Chapter 2

## Background

The Probing Radio Intensity at high-Z from Marion (PRI<sup>Z</sup>M) global signal experiment is the main inspiration for the complementary interferometer Array of Long Baseline Antennas for Taking Radio Observations from the Sub-antarctic - Exploratory Gizmo on the Ground (ALBATROS-EGG). Both projects are located on Marion island in a radio quiet zone halfway between South Africa and Antarctica.

### 2.1 The PRI<sup>Z</sup>M experiment

The Probing Radio Intensity at high-Z from Marion (PRI<sup>Z</sup>M) experiment aims to observe the 21-cm from neutral hydrogen, but redshifted to frequencies from 30-200 MHz which correspond to the observing frequency range of PRI<sup>Z</sup>M [5]. At this redshift is the epoch of cosmic dawn between  $6 < z < 27$  during which the very first stars were formed [7].

The motivation for this experiment is to verify the theoretical predictions in Figure 2.1 for the global signal and to measure the brightness temperature from the formation of the first galaxies to the period of reionization. A recent detection of the 21-cm signal measured by the EDGES experiment at 78.1 MHz, within the frequency range of the PRI<sup>Z</sup>M experiment, showed a surprising result [20]. As it was stated in the discovery paper, the profile of the 21-cm line from early stars was predicted by theory, while on the other hand, the amplitude of the observed feature was twice the maximum theoretical limit [20]. This implies that the primordial gas is colder or that background radiation temperature is hotter than predicted [20]. Since this detection is unique for the moment, the goal is to replicate the findings using a different instrument at a different location.

Observing the 21-cm line over these frequencies is a great challenge mainly due

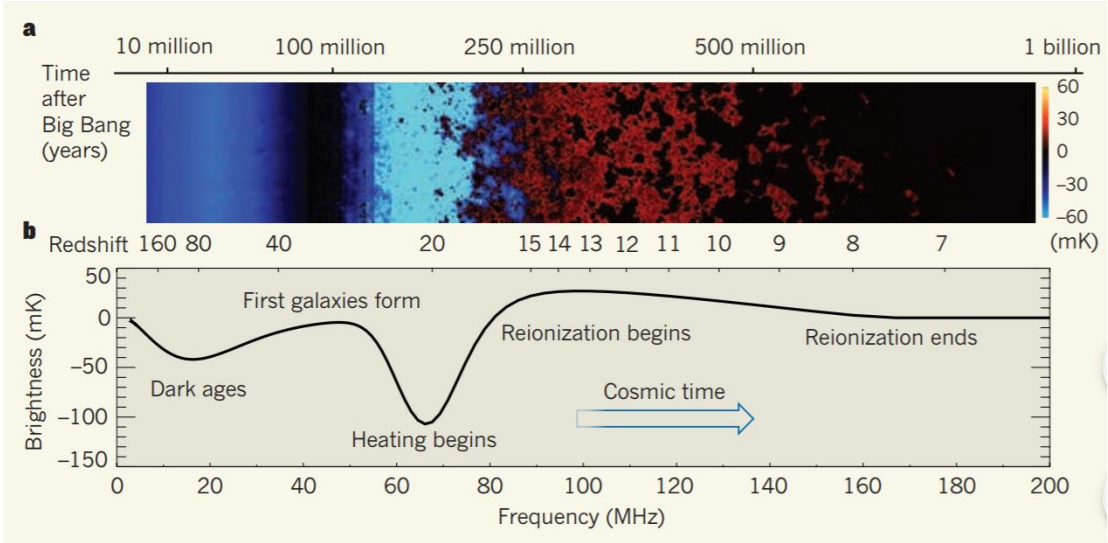


Figure 2.1: Sky brightness of the 21-cm signal as a function of redshift and observation frequency [7]: a) 21-cm tomography measuring the temperature brightness variations, b) global signal temperature brightness variations and the respective events they represent.

to the radio frequency interference (RFI) which is mainly caused by human-made devices and satellite communication. For this reason, the project was located on Marion island midway between South Africa and Antarctica located in a very radio quiet region.

The PRI<sup>Z</sup>M instrument is composed of two antennas centered at 70 MHz and 100 MHz respectively, covering a combined frequency range of 30-200 MHz [5]. While this instrument's research goals are different than the one for ALBATROS, the instrumentation is similar and both experiments share the same location. The main distinction is that PRI<sup>Z</sup>M is a global signal experiment thus requiring few antennas, while the ALBATROS experiment is going to be doing sky mapping (tomography). The later will thus require a high resolution and will therefore involve interferometry. Figure 2.2 shows the site used for both PRI<sup>Z</sup>M, and ALBATROS-EGG.

## 2.2 ALBATROS-EGG experiment and ALBATROS Interferometer

The Array of Long Baseline Antennas for Taking Radio Observations from the Sub-antarctic - Exploratory Gizmo on the Ground (ALBATROS-EGG) experiment is essentially a tomography low frequency extension of the PRI<sup>Z</sup>M global

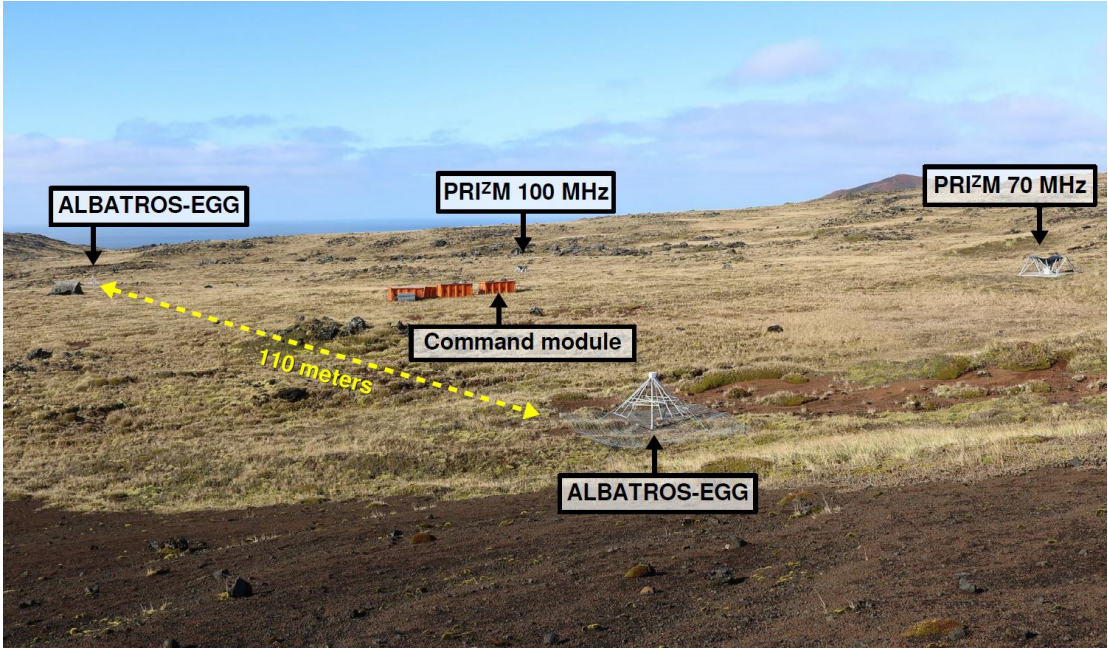


Figure 2.2: Experimental setup of the PRIZM and ALBATROS-EGG experiment on Marion island [8]

signal experiment. Two Long Wavelength Array (LWA) antennas with an operational frequency of 5 – 90 MHz, but with an actual capacity as low as 1.2 MHz were installed on Marion island to map the sky at frequencies just after the epoch of the Cosmic Microwave Background (CMB) formation, at the epoch of the Dark Ages at redshift  $1100 > z > 30$  [17] as shown previously in Figure 2.1.

The low RFI on Marion island suggests that with the addition of more antennas combined with an observation run during a solar minimum, it will be possible to improve on previous observations. The state of the art sky mapping at such low frequencies dates back to 1968 [9] as shown in 2.3. As shown in Figure 1.8, the ionosphere becomes more transparent at low frequencies during solar minima [9] which is why timing is crucial for observation. Luckily, the period for this cycle is slightly more than a year for Marion. The difference in plasma frequency in the ionosphere is almost of a factor of two. Despite the effort on minimizing noise, these frequencies are expected to be dominated by galactic noise. However, the characterization of the latter is also equally important for the development of further low frequencies mapping experiments.

After the deployment of the ALBATROS-EGG experiment, the preliminary results were promising enough to start designing for an expansion towards more antennas and creating an interferometer capable of mapping the whole visible sky at these latitudes. This projected interferometer is called ALBATROS and it is expected to be fully deployed within the next few years. This interferometer

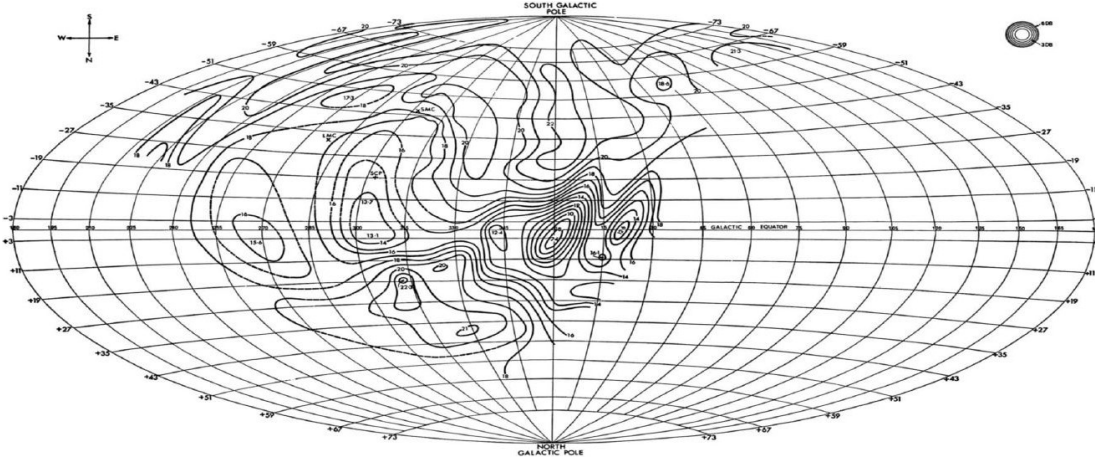


Figure 2.3: State of the art mapping at 2.1 MHz [9]

with operational frequencies of 1.2-81 MHz will be composed of nine autonomous LWA antennas located at the nine huts on the island as shown in Figure 2.4. The combined beam has been simulated to have a FWHM of 8 arc minutes at 5 MHz [8]. Given that each antenna will be located several kilometers away from its nearest neighbor, the signals won't be correlated in real time, but the data will rather be written to disk and then correlated offline. This is possible when the data is precisely time-stamped before it's stored. Given that the baseband data output is small at such low frequencies, the storage through hard drives is actually feasible.

## 2.3 ALBATROS Instrumentation

All ALBATROS autonomous stations will be identical and spread out across the island to give very long baselines. Therefore, they need to be lightweight enough to be transportable by hikers. Each station will be composed of:

1. LWA antenna optimized for 5-90 MHz.
2. Active balun ensuring the signal is delivered at the right amplification without reflections at the load.
3. Radio frequency tight enclosure containing the back end electronics.

In the final design, each autonomous station will be powered through solar panels [21]. However, this has not yet been implemented on the current ALBATROS-EGG prototype. This being said, the current design uses two Honda generators to charge the 12V power supply connected to all the back end electronics.

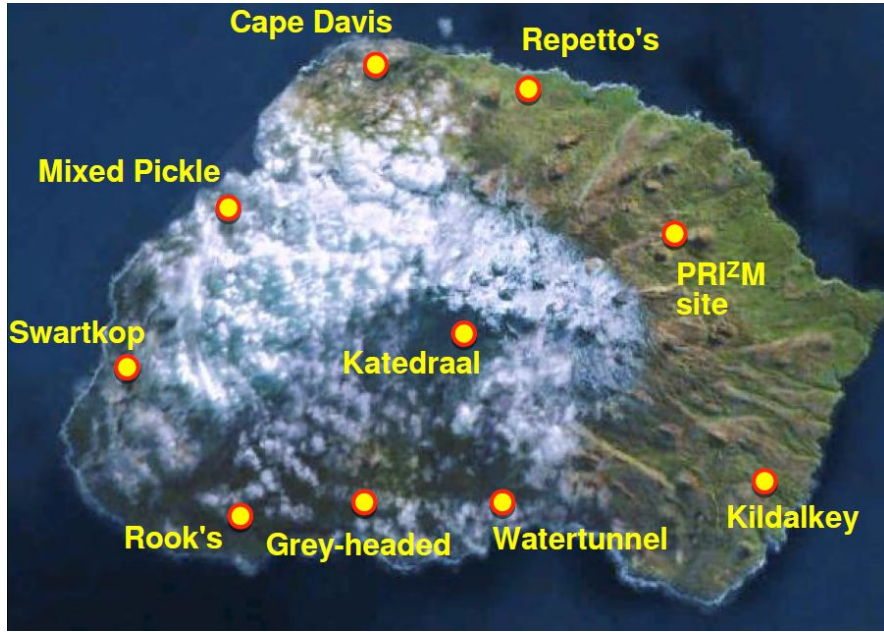


Figure 2.4: The projected distribution for the ALBATROS interferometer will correspond to the current hut distribution on Marion island [8].

### 2.3.1 LWA antenna

The Long Wavelength Array (LWA) antenna is the same as the one used for LWA-1 in New Mexico [15]. This type of antenna is optimized for low frequencies between 10 – 88 MHz [15]. The architecture of the antenna as seen in 2.5 is composed of a 3 x 3 m wire mesh with 10 x 10 cm spacing [15]. The purpose of this grid is to discourage absorption of the signal into the ground, but also to prevent the environmental condition of the ground (dry or wet) to affect how much is absorbed and how much is reflected [22]. For the antennas, they are two dipole antennas shaped like a bow-tie angled at 45° with respect to the ground [15] as it can be seen in Figure 2.5. Each dipole has smaller horizontal segments in order to increase the frequency range to higher frequencies. The shape and orientation of this dipole is designed such that a spherical and omnidirectional beam pattern is produced [8]. Due to the contribution of the wire mesh, the beam pattern is directed upwards instead of being fully symmetric and capturing the ground’s noise with the same gain.

The main challenges with the antenna design as well as with the array design at low frequencies are the variable and inhomogeneous effects of the ionosphere as well as the galactic noise. The signal from our own Milky Way galaxy is a significant variable to consider when calculating the sensitivity of the overall array. This influences the integration time as well as the calibration of the interferometer.



Figure 2.5: The LWA antenna on Marion island with the two dipoles shaped like a bow-tie hanging above the wire mesh layed on the ground [8]

### 2.3.2 Active Balun

Each LWA dipole is connected to an active balun which has a balanced input impedance of  $100 \Omega$  [15]. The balun is a device that converts a balanced signal to an unbalanced signal. The main purpose of the balun is to prevent coupling between the dipole and the coaxial cable feeding the signal to the rest of the signal processing components so that the coaxial cable does not act like an antenna. Additionally, the balun is used to provide sufficient amplification to compensate for any loss within the transmission line as well as to insure impedance matching with the coaxial cable to avoid reflections of the signal. The inner workings of the balun are shown in 2.6. Each dipole signal is first amplified and then coupled through the hybrid coupler, a four-port device that introduces a  $180^\circ$  phase-shift between the two signals to isolate them from one another. The output signal is passed through an RFI filter which is simply a bandpass filter which eliminates unwanted frequencies. Finally, the signal is amplified again and a bias tee (more details in 2.4.2) is used to both power the LWA balun and to match the signal to the impedance of the coaxial cable which is typically  $50 \Omega$ . This last step is very important so that the signal does not reflect back into the front end electronics because of impedance mismatch.

## 2.4 ALBATROS Signal Processing

Prior to the signals being correlated together, the data acquired by each station is filtered, digitized, time stamped, and written to disk. This sub-section provides further information about the signal processing done by the back end electronics

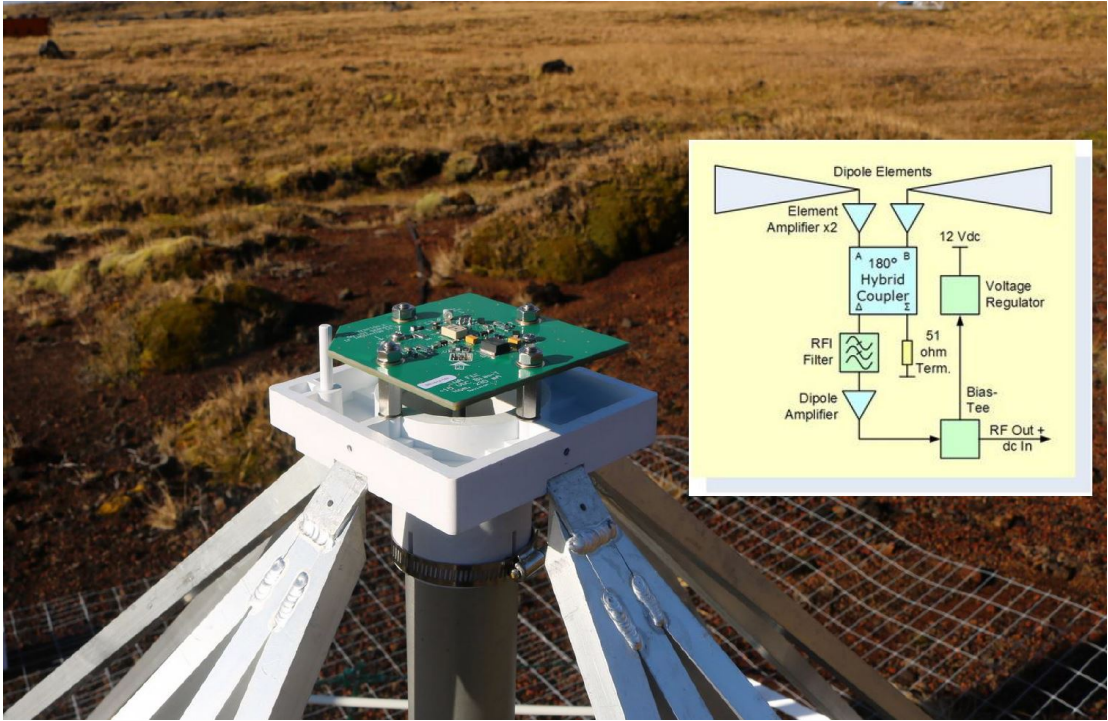


Figure 2.6: Active balun as located on the LWA antenna and a schematic illustrating the inner workings of the active balun [8]

from signal acquisition to correlation between each station.

### 2.4.1 Signal Processing

In the case of the ALBATROS-EGG experiment, once the signal has been acquired by the 35 dB balun as described previously, it is sent along a coaxial cable towards the aluminum enclosure which acts like a Faraday cage shielding the antennas from the electromagnetic fields generated by the back end electronics. The signal is then passed through the bias tee which insures that only the AC signal goes through while blocking any DC signal. The bias tee acts like an ideal capacitor and an ideal inductor by passing only AC or passing only DC. It is an active device, therefore it needs a bias DC voltage to work over a given frequency range.

As shown in the schematic in Figure 2.7, once the analog signal collected by the LWA antennas has been acquired, it goes through both a high pass filter and a low pass filter to fix the signal range to 1.2 – 81 MHz. An amplifier then increases the amplitude of the signal by 20 dB before passing it to the SNAP board for cross-correlation and digitization. In the ALBATROS-EGG prototype, two antennas were used and their signals were cross-correlated directly. Each LWA antenna has

two outputs from the balun which requires four signal processing chains prior to their input into the SNAP board. However, the ALBATROS autonomous stations will have one LWA antenna for every back end enclosure in addition of having their signal correlated offline. These major changes alter the number of inputs and the components present in the enclosure.

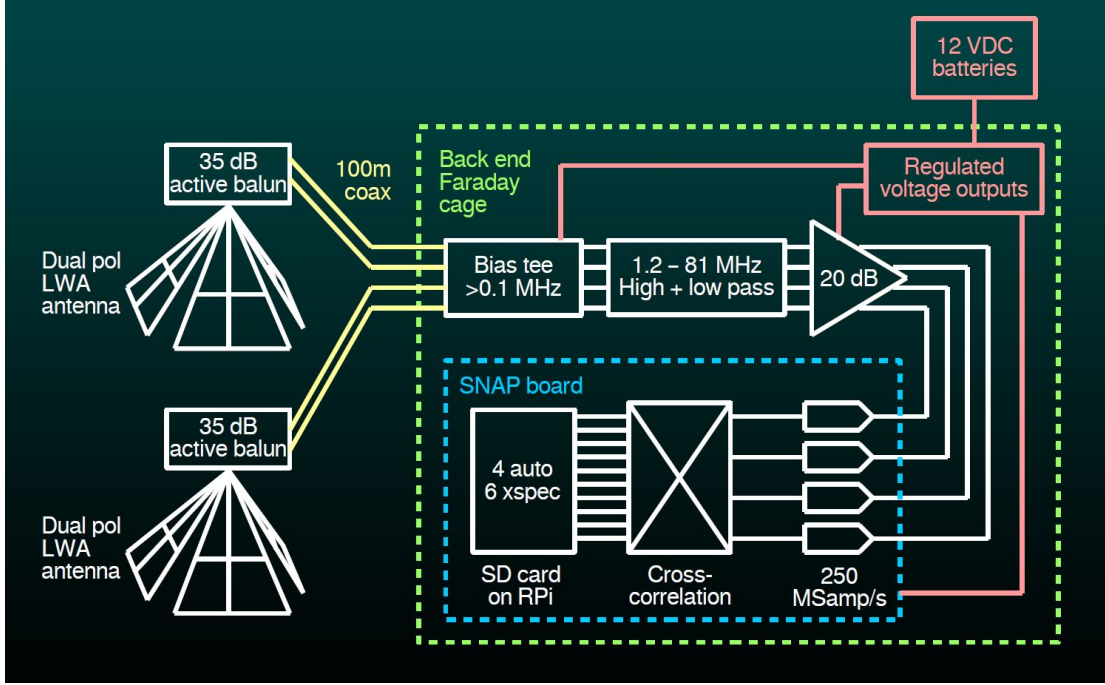


Figure 2.7: ALBATROS-EGG simplified schematic for the back end electronics [8]

#### 2.4.2 Back end electronics

The back end electronics are all contained in a light weight aluminium enclosure which has been the main topic of this work. The enclosure contains all the essential components (see Figure 2.8) for the signal processing, the precise time stamping that will ensure correlation of the signals during offline processing, and the storage of the data.

**SNAP board:** The Smart Network ADC Processor (SNAP) board is an open-source platform designed for digitizing and compressing analog signals (see Figure 2.9). The SNAP board has been developed specifically for this type of applications by CASPER for the Hydrogen Epoch of Reionization Array (HERA) experiment [10]. In addition to its relevant heritage, the SNAP board was also designed to be widely modular and compatible. It is an essential piece of equipment that allows an input of a radio frequency (RF) signal and an Ethernet output by using the

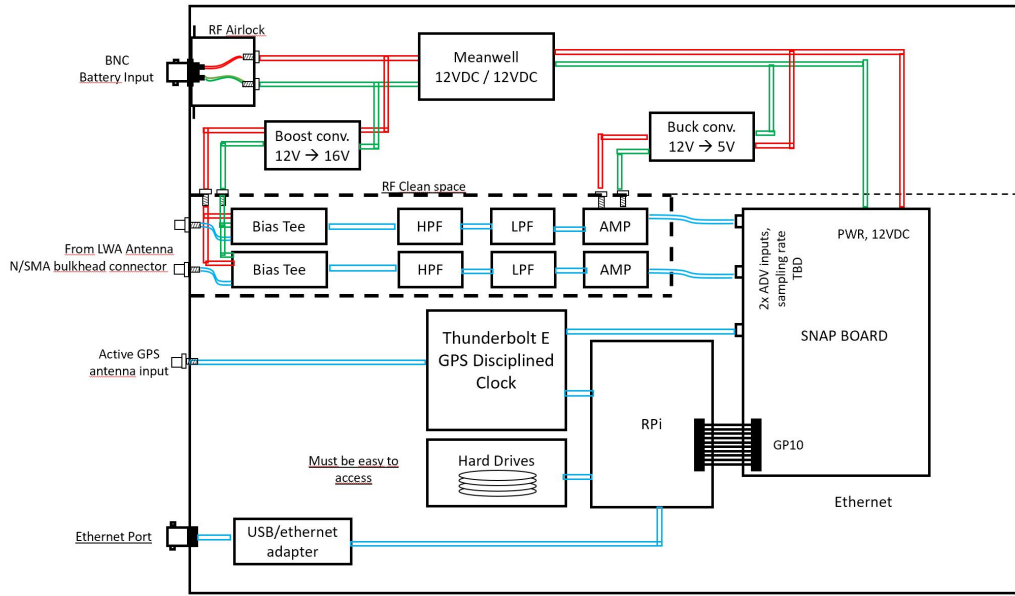


Figure 2.8: ALBATROS back end electronics wiring diagram. This schematic shows the new components with respect to the previous ALBATROS-EGG experiment.

Ethernet 10 Gb protocols. It also allows for a connection with a Raspberry Pi computer, which is also used as part of the ALBATROS back end electronics.

**Bias Tee:** The Bias Tee allows us to superimpose a DC voltage on top of analog signals so that the remote amplifiers on each antenna can be powered without the need for an additional power cable. The Bias Tees are located in the RF shielded part of the enclosure since they take part in the signal processing prior to digitization within the SNAP board. One Bias Tee is connected after the High Pass Filter (HPF) and the Low Pass Filter (LPF). The ZFBT-4R2GW-FT could be used for a frequency range between 0.1 – 4200 MHz.

**High Pass Filter:** The high pass filter used here is the ZFHP-1R2-S+ which has a range of 1.2 – 800 MHz. Its function is to block any frequencies which may be lower than 1.2 MHz.

**Low Pass Filter:** Similarly as the HPF, the LPF SLP-90+ is blocking any frequencies higher than 81 MHz. These filters ensure that no signals outside of this ranged are passed to the SNAP board.

**Amplifier:** This component amplifies the voltage of the signal by 20 dB. There are two different ones that were used up to now: ZX60-V63+ / ZX60-33LNR-S+ or ZFL-500+.

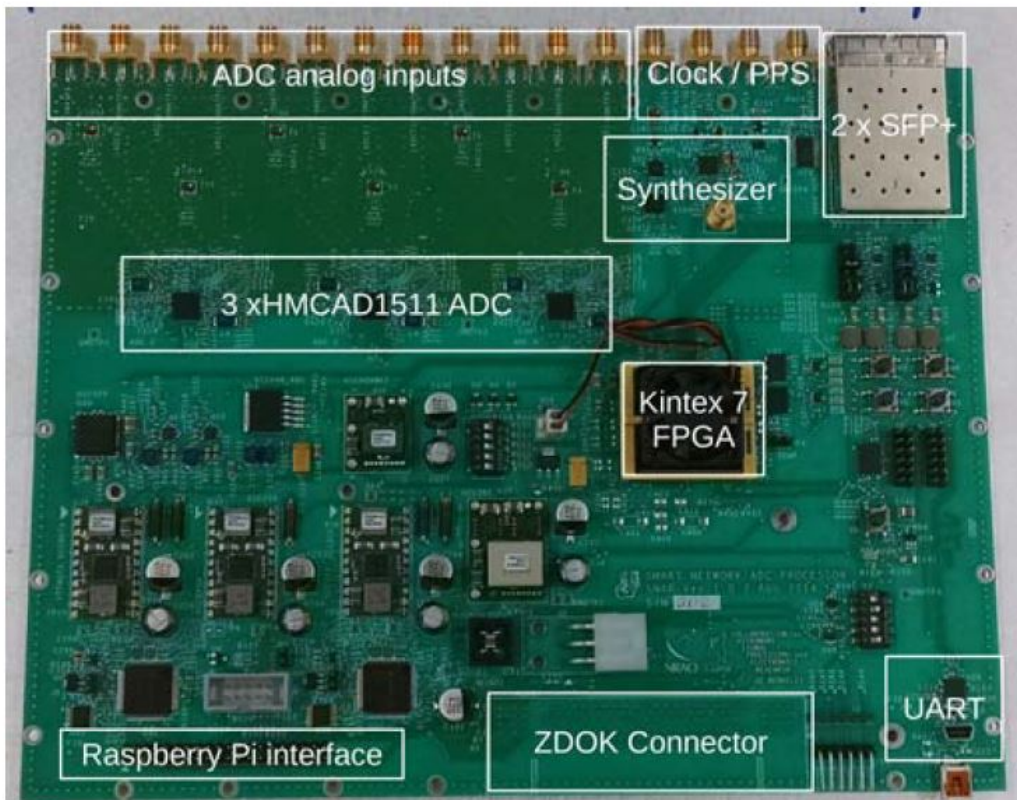


Figure 2.9: This figure illustrates the main features of the SNAP board. For the purpose of this experiment only two ADC analog inputs, one clock/PPS input, and the Raspberry Pi interface will be used. [10]

**GPS Disciplined Clock:** The Trimble Thunderbolt E GPS Disciplined Clock is used to provide the exact time to the SNAP board and the Raspberry Pi onboard computer. This clock has a GPS receiver to synchronize time and location wirelessly. The overall system generates a timestamp for the data with nanoseconds accuracy in addition of being very stable [23]. This component has been a major upgrade compared to previous GPS and clock modules used in ALBATROS-EGG.

# Chapter 3

## Enclosure Design

One of the biggest priorities when building a telescope is to ensure that the instrument doesn't measure itself instead of capturing an astronomical signal. To decrease the level of noise in the system several measures can be applied: cooling the electronics to cryogenic temperatures, choosing a remote location, or shielding the noise produced by the electronics. This section treats the latter point by proposing an improved and flexible enclosure design that isolates the signal processing components from the rest of the system. In this section, a few previous designs along with the improved version will be presented, the layout of the electronics inside will be revised and gaskets for further shielding are discussed, as well as the main software used for this project.

### 3.1 Previous Enclosures

The SNAP enclosure is where the signal is treated before it is stored as data. During the development of the ALBATROS-EGG prototype several versions of this enclosure were developed. However, for the deployment of the ALBATROS project all ten stations composing the array shall be identical and properly shielded to avoid contamination of the data.

The first SNAP enclosure was meant to hold the electronics which were being tested. No 3D drawing was made or shielding between the components was done at this stage. The holes for the connectors were drilled manually. The next version of the SNAP enclosure (Figure 3.1) was made using Computer-Aided Design (CAD) software. While the enclosure served its purpose, several improvements needed to be done for the ALBATROS project. Gaps in the corners and at the junction of the brackets, as well as no shielding at the connector level was still a problem in terms of RF tightness.



Figure 3.1: ALBATROS-EGG SNAP Enclosure showing gaps at the corners and signal processing chains containing the amplifiers within the same space as the SNAP board.

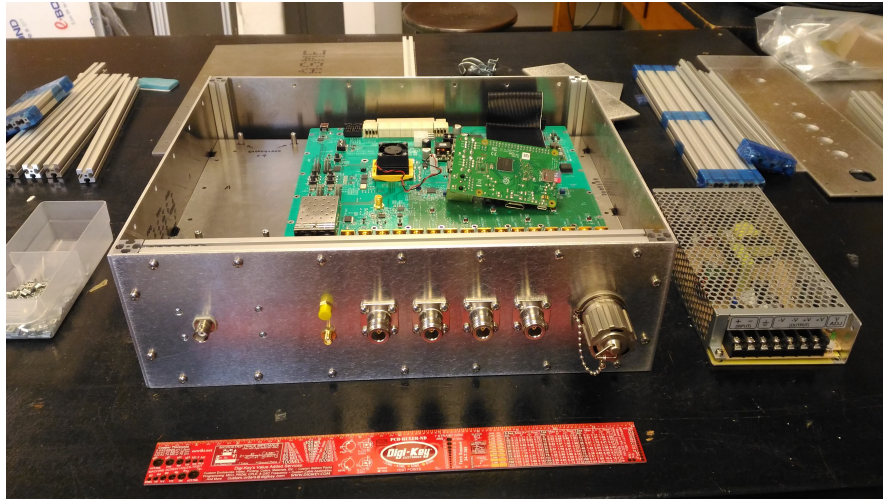


Figure 3.2: Improved ALBATROS-EGG enclosure design with four inputs and shielded connectors.

The latest version of the ALBATROS-EGG SNAP enclosure (Figure 3.2) solved the previous issues through the addition of shielded connectors and the use of square aluminum extrusions. While this was a major improvement upon the previous design, the ALBATROS version requires two inputs for the antennas instead of four. Also, a shielded section of the enclosure needed to be added in order to create another Faraday cage around the signal processing part of the electronics. These additional requirements lead to the development of the ALBATROS SNAP enclosure.

## 3.2 Improved Design

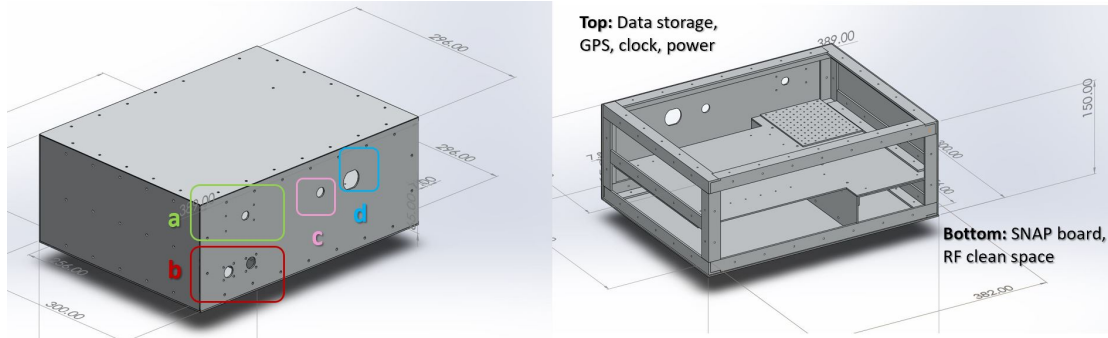


Figure 3.3: New ALBATROS enclosure design: (a) power input, (b) LWA antennas input, (c) GPS receiver input, and (d) Ethernet input.

The major improvement with the new CAD design is the addition of a radio frequency clean space where all the filters and bias tees will be housed (Figure 3.4). The bracket junctions are also precisely designed to fit in one another without any gaps at the corners (Figure 3.3). The full 3D design was made using the SolidWorks software. The modularity of this tool allowed to make a flexible design with driven patterns to facilitate the accommodation of future components. The dimensions of this enclosure are slightly taller than the previous version with the purpose of adding more hard drives and house keeping components to improve performance. The dimensions of this version are 38.9 x 30.0 x 15.3 cm making it transportable to various locations using a backpack, another requirement given the difficult terrain and harsh climate on Marion island. The front side of the enclosure is where everything is connected: the two N-connectors carrying the signal from the antenna, the power cable, the Ethernet port, and the SMA connector for the GPS (Figure 3.3). On the top side of the shelf a grid is placed held by stand-offs to fix the different voltage converters. The middle shelf has an indentation of 3 cm on both sides to allow easy access to connections between the top electronics and the SNAP board underneath. The overall design was done such that any panel could be unscrewed from the outside without affecting the remaining structure. This way the house keeping and data storage components can be accessed from the top while the signal processing side of the electronics can be accessed from the bottom (more details in section 3.3).

In the Figure 3.4, the bottom half of the enclosure is shown where the RF shielded section is located. A grid that will be held in place by stand-offs allows for personalized arrangement of the filters. The holes of the SNAP board which will be held by stand-offs in the shelf are located such that the Raspberry Pi connection is close to the front panel and the Raspberry Pi itself.

The bottom view in 3.5 shows more clearly the location of the Raspberry Pi

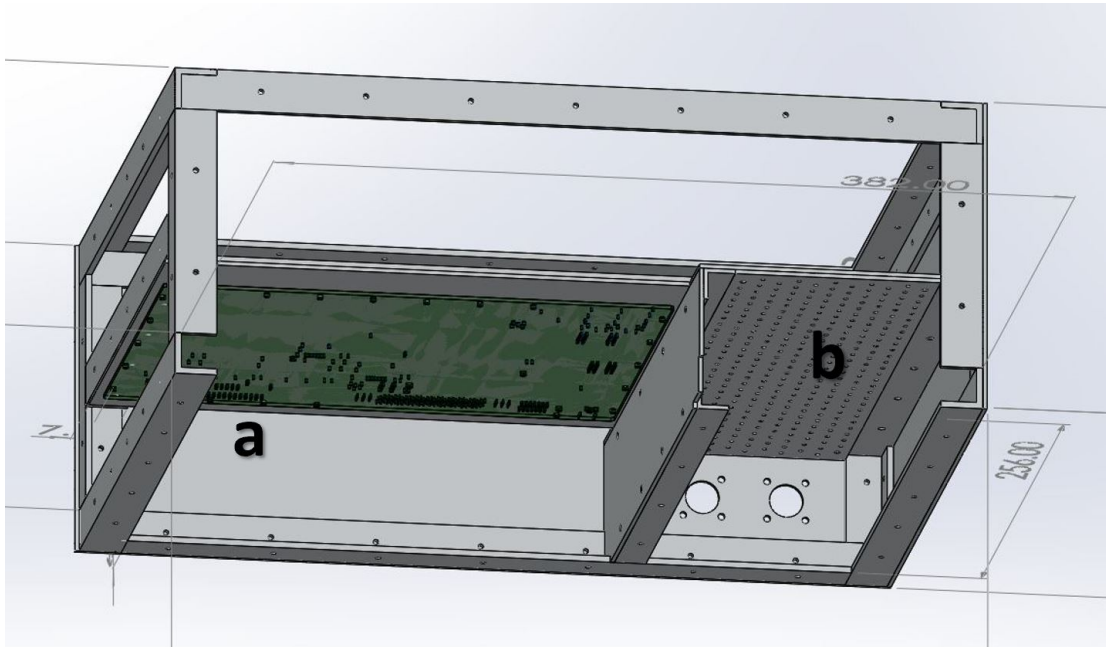


Figure 3.4: Bottom-back view of the ALBATROS enclosure showing the SNAP board location (a) and the RF clean space (b).

connection to the SNAP board in the bottom right corner facing the front panel of the enclosure. The other half is meant for the RF clean space with dimensions of 13.3 x 29.6 x 6.1 cm.

The exploded view (Figure 3.6) shows all 26 parts necessary for the assembly excluding the M2.5 and M3 standard screws and stand-offs. All components are made from aluminum with the sheets being 2 mm thick and the right angle brackets being 3 mm thick. The desired manufacturing process would be through laser cutting.



Figure 3.5: Bottom view of lower half of the ALBATROS enclosure showing the location of the Raspberry Pi connection in the bottom-right corner.

### 3.3 Components Layout

The entire enclosure design is based on the size and connections of each component. The ALBATROS enclosure requires additional space to house one or several external hard-drives to save all the data. For this reason it is slightly larger than the previous version. Figure 3.7 shows the current layout of the components.

The main components contained in the enclosure are:

1. SNAP board
2. Bias tees (x2)
3. High pass filters (x2)
4. Low pass filters (x2)
5. Amplifiers (x2)
6. Raspberry Pi
7. Voltage converters (x4)
8. GPS & clock
9. 5T hard drive (x2)

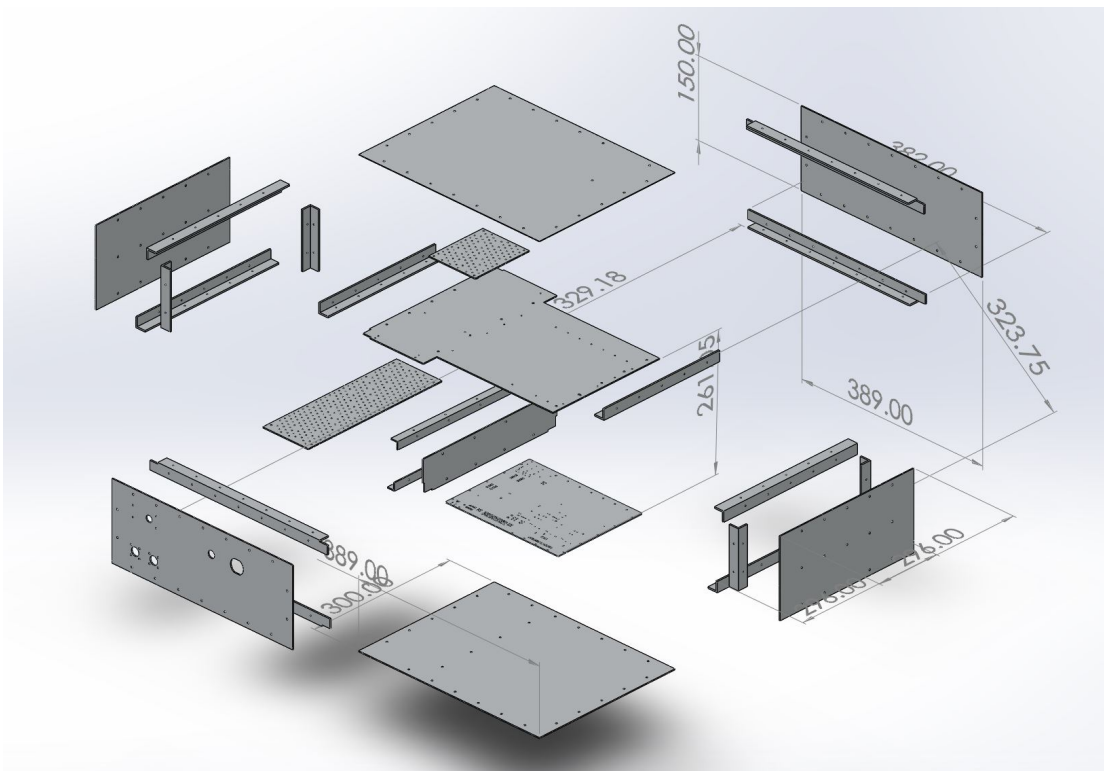


Figure 3.6: Exploded view of the ALBATROS new enclosure

10. RF shield box for the power cable
11. 12V power supply
12. Low voltage regulator

The main reason for which this design would be modified in the future is as a consequence of the components choice. If the components remain the same but the layout is different, the front panel holes may vary in position. Also, if many more hard drives are added to the design, then the height of the enclosure could be changed to stack several hard drives on top of each other. Since the layout of the components is not finalized for the future, then no holes for the standoffs can be finalized either. For an even more flexible version of the top part of the shelf, one may use the same hole pattern as on the grid for the voltage converter and apply it to a copy of the middle shelf part creating a full grid for the entire shelf.

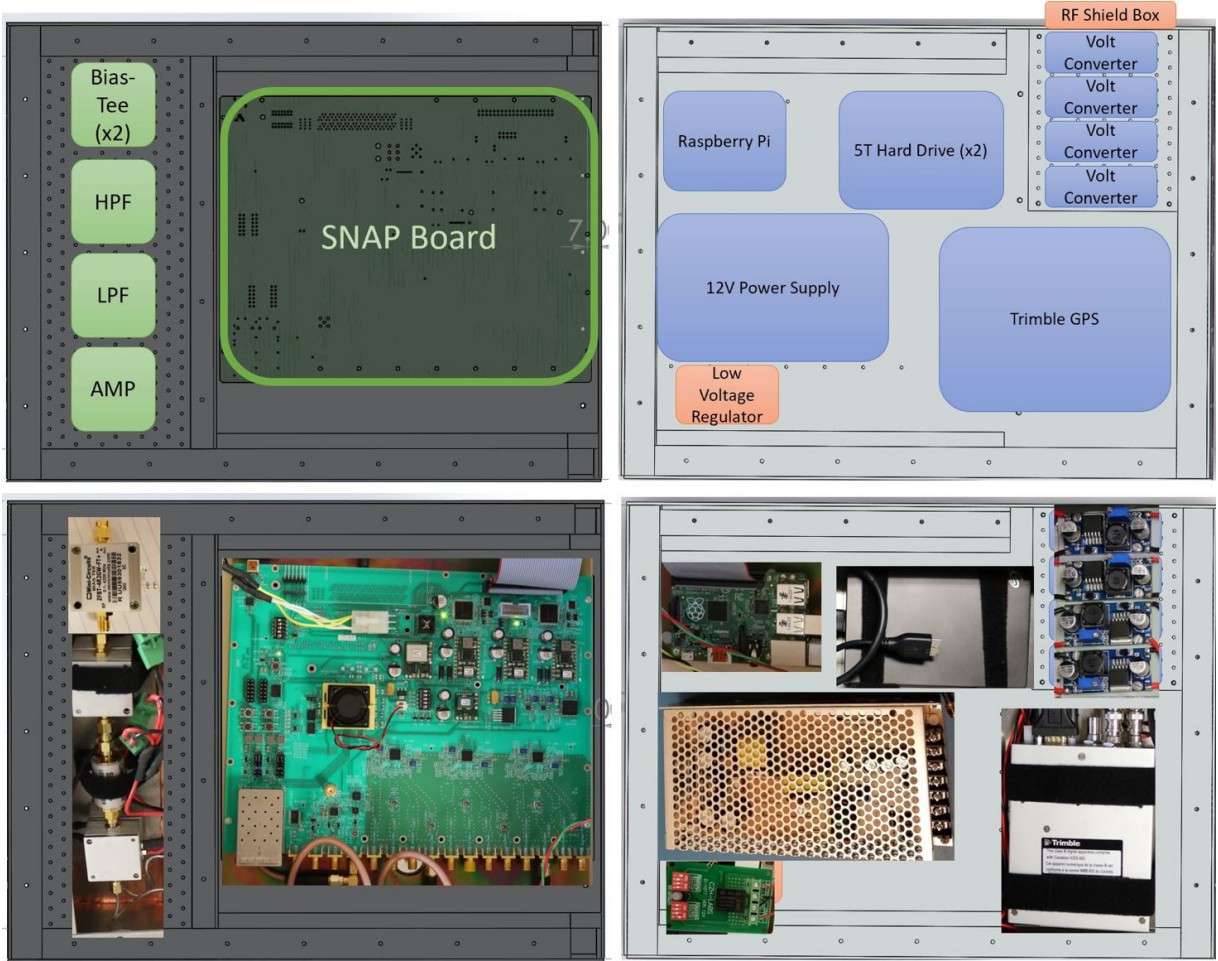


Figure 3.7: Component layout and the corresponding photo montage of the bottom part of the shelf and top part of the shelf respectively (not to scale) assuming the top of the picture is the front panel where all the inputs are. The axis of symmetry is along the y-axis between the two pictures.

### 3.3.1 Enclosure Shielding Effectiveness

To ensure the effectiveness of the RF clean space designed within the enclosure, the shielding effectiveness is calculated below according to NASA's *Design Guidelines for Shielding Effectiveness, Current Carrying Capability, and the Enhancement of Conductivity of Composite Materials* [24]. The total effectiveness in dB can be calculated by dividing the problem into the contributions from the choice of material, the apertures in the metal sheets, and the discontinuities at the edges of the enclosure.

**Shielding effectiveness due to the material:**

Shielding effectiveness depends on the conductivity and the thickness of the material used for the enclosure. At low frequencies, this attenuation is lower than at higher frequencies. The shielding effectiveness through an infinite sheet of material is defined by Equation 3.1.

$$SE = A_{dB} + R_{dB} + B_{dB} \quad (3.1)$$

$SE$ : Shielding Effectiveness

$A_{dB}$ : Attenuation due to absorption

$R_{dB}$ : Loss due to reflection

$B_{dB}$ : Rereflection correction

For a plane wave, the later quantities are defined in Equations 3.2, 3.3, and 3.4, where  $\eta_0$  is the intrinsic impedance of free space  $\eta_0 = 377\Omega$ ,  $\eta_s$  is the intrinsic impedance of the material  $\eta_0 = \sqrt{\frac{2\pi f\mu_0}{\sigma}}$ , and  $\delta$  is the skin depth  $\delta = \frac{1}{\sqrt{\pi f\mu_0\sigma}}$ . Note that  $f$  is the frequency,  $\sigma$  is the conductivity of the material,  $\mu_0$  is the permeability in free space, and  $t$  is the thickness of the metal sheet or barrier.

$$R_{dB} = 20 \log \frac{\eta_0}{4\eta_s} \quad (3.2)$$

$$A_{dB} = 20 \log e^{\frac{t}{\delta}} \quad (3.3)$$

$$B_{dB} = 20 \log |1 - e^{\frac{t}{\delta}}| \quad (3.4)$$

In the case where the source is located at a shorter distance than the signal's wavelength, near field shielding applies. The loss due to reflection becomes Equation 3.5, where  $Z_w$  is the wave impedance.

$$R_{dB} = 20 \log \frac{Z_w}{4\eta_s} = 20 \log \frac{2\pi\mu_0 r}{4\eta_s} \quad (3.5)$$

Calculating the shielding effectiveness using the near field equations in the case of the RF clean space, we find that the attenuation for a 2mm Aluminum sheet located at 1 cm from the source is very high (Figure 3.8). In practice, any number that is above 100 dB means that the material is almost impenetrable [25]. In the case of Aluminum, which is a very good material to use for shielding, the performance decreases only at 0.01 mm thickness keeping the distance from the source constant (Figure 3.10). We find that even for the source located at 10 m

away using the plane wave equation (Equation 3.2), the thickness of the material provides very good attenuation (Figure 3.9).

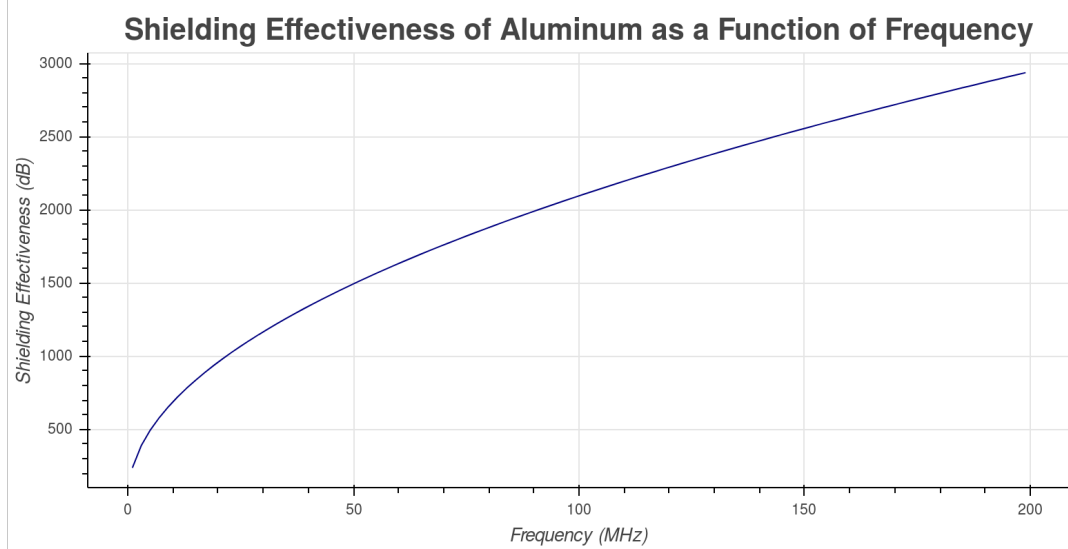


Figure 3.8: Shielding effectiveness of a 2mm aluminum sheet with the source located at 1 cm away.

#### Shielding effectiveness due to holes and edges:

The RF clean space contains several holes for the screws as well as discontinuities at the edges where the aluminum panels meet. The shielding effectiveness adds up for apertures as in resistors in parallel:

$$\frac{1}{SE_{total}} = \frac{1}{SE_1} + \frac{1}{SE_2} + \frac{1}{SE_3} + \dots \quad (3.6)$$

For each hole the shielding effectiveness is:

$$SE_{dB} = 99 - 20 \log(L f_{MHz}) + SE_{shadow} + 30 \cdot \frac{d}{L} \quad (3.7)$$

For each slit the equation is:

$$SE_{dB} = 97 - 20 \log(L f_{MHz}) + 20 \log(1 + \ln \frac{L}{S}) + SE_{shadow} + 30 \cdot \frac{d}{L} \quad (3.8)$$

Both equation 3.7 and equation 3.8 require a quantity  $SE_{shadow}$ . This shadow shielding effectiveness is due to the interference pattern of waves passing through

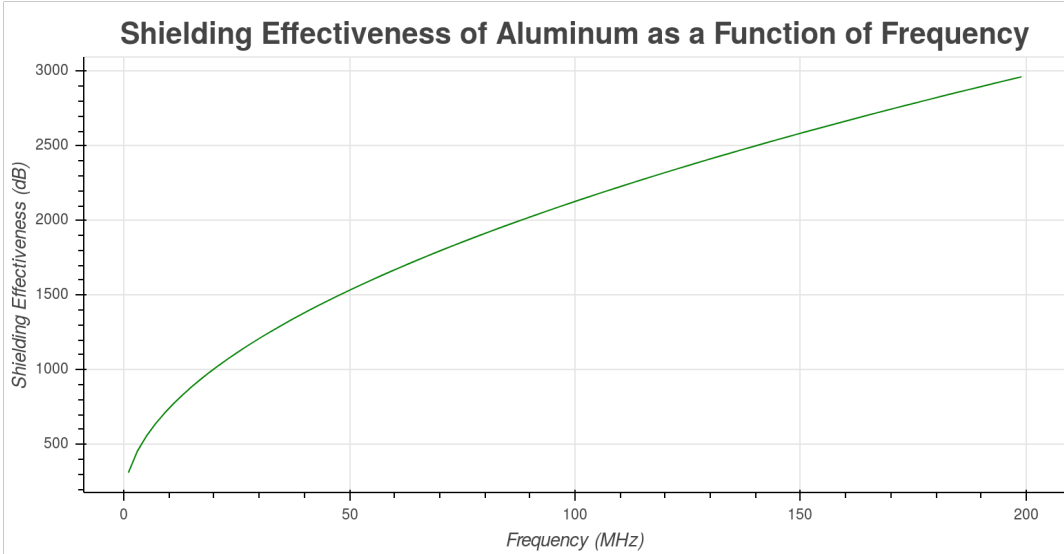


Figure 3.9: Plane wave shielding effectiveness of a 2 mm aluminum sheet with the source located at 10 m away.

the aperture and bouncing back on the walls of the enclosure. This value is defined from the ratio of the slit to box dimensions in mm (the length or diameter  $L$ , the width  $S$ , and the thickness  $d$ ). In a table found in the *Design Guidelines for Shielding Effectiveness* [24], the value for the proportions of the RF clean space is reported to be approximately 6 dB, while for the entire enclosure this value was 3 dB.

#### RF Clean Space:

To estimate the maximum loss from the apertures, all the holes are considered to be exposed without screws and the edges are considered without brackets blocking them. In other words, this is the maximum loss due to the holes and edges. Figure 3.11 shows the result for the RF clean space when considering the screw holes to be uncovered and a 2mm gap at each edge. It was calculated that the longest edges have the largest effect on the resulting shielding effectiveness.

Number of apertures	Thickness	Dimensions of Aperture
16	4 mm	2.50 mm
18	5 mm	2.50 mm
8	2 mm	2.05 mm
4	2 mm	115 x 2 mm
4	2 mm	296 x 2 mm
4	2 mm	43 x 2 mm

Table 3.1: List of apertures considered for the calculations of the RF clean space including dimensions and thickness of the material at that location.

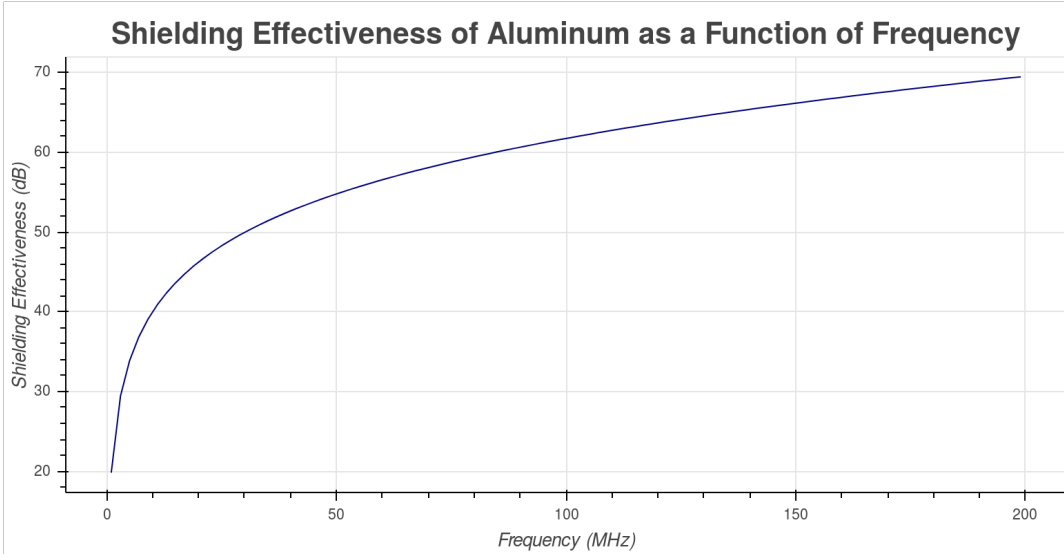


Figure 3.10: Shielding effectiveness of a 0.01 mm aluminum sheet with the source located at 1 cm away.

Taking the dimensions from Table 3.1 and substituting into Equation 3.6, we find that the total shielding effectiveness is between approximately 25 – 60 dB for the frequency range of ALBATROS.

#### Full Enclosure:

Similarly as for the RF clean space, all holes and edges for the entire enclosure were considered to be uncovered to take into account the worst case scenario. Table 3.2 shows the dimensions and number of apertures. The resulting Figure 3.12 shows a lower performance than the one for the RF clean space due to the longer edges which were calculated as slits.

Number of apertures	Thickness	Dimensions of Aperture
111	5 mm	3.40 mm
1	2 mm	6.9 mm
4	2 mm	153 x 2 mm
4	2 mm	300 x 2 mm
4	2 mm	389 x 2 mm

Table 3.2: List of apertures considered for the calculations for the full enclosure including dimensions and thickness of the material at that location.

#### Total shielding effectiveness:

To constrain the attenuation range, the lowest shielding effectiveness for the material and the lowest shielding effectiveness for the apertures must be taken into

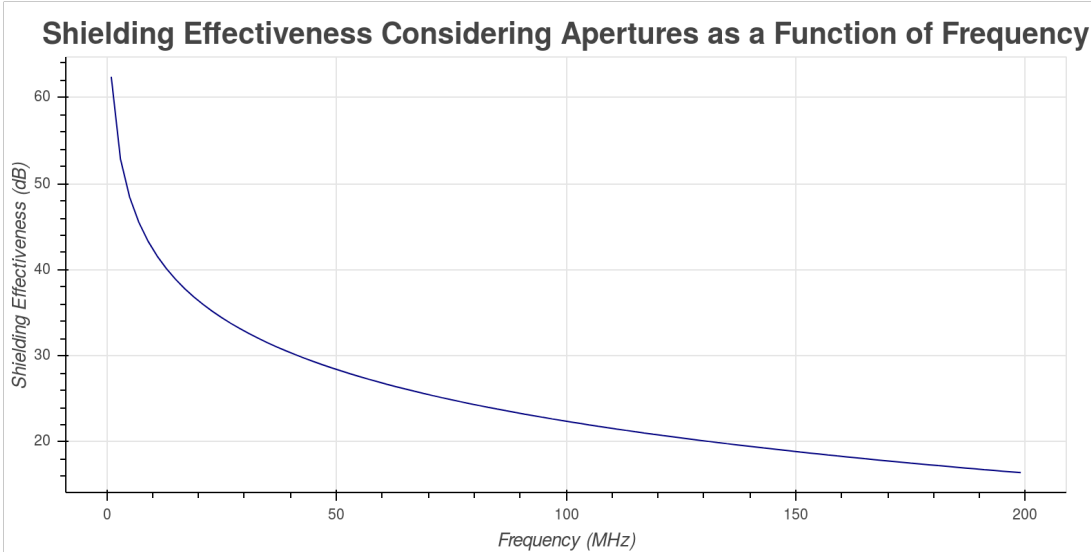


Figure 3.11: Shielding effectiveness considering holes without screws and edge gaps of 2mm.

Location	Required Attenuation	Estimated Attenuation
Inside enclosure	35 dB	17.5 dB
Inside RF clean space	55 dB	24.2 dB

Table 3.3: Required shielding effectiveness compared to the estimated value

account. The reason for this is that the thickness and conductivity of the material limit the lower frequencies, while the dimensions of the apertures limit the higher frequencies. Since the material limit is above 100 dB due to the thickness of the Aluminum sheets, the overall attenuation limit is taken to be the one for the apertures at 81 MHz. Table 3.3 shows how the worst case scenario calculations compare to the required shielding given that the full signal in the box escapes. In reality however, these gaps won't be there because of the brackets and the fact that the panels will be tightly screwed. Therefore, the real effectiveness will approach the material effectiveness rather than the aperture effectiveness.

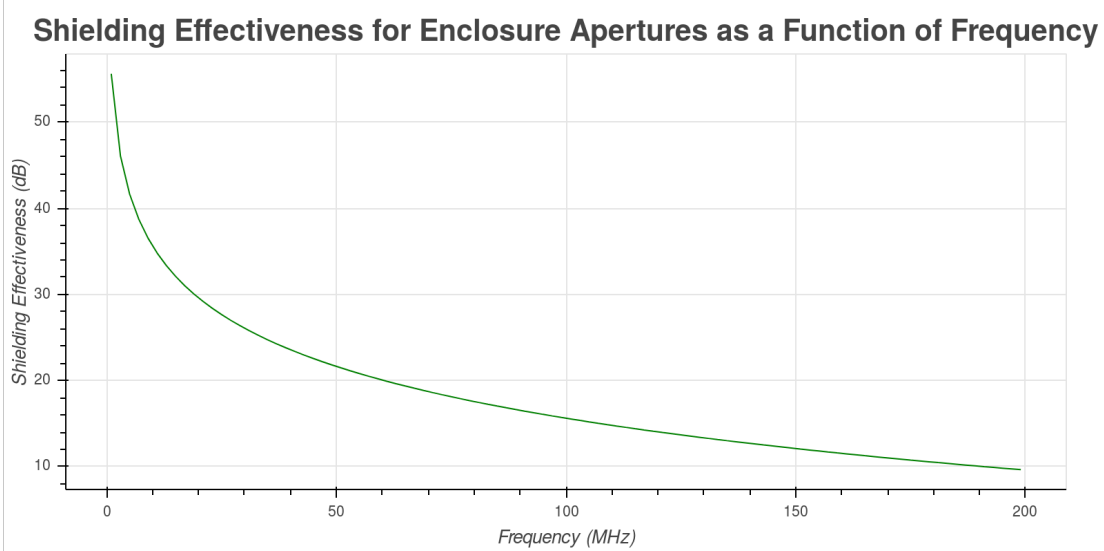


Figure 3.12: Shielding effectiveness for the entire enclosure considering holes without screws and edge gaps of 2mm.

### 3.4 Gasket Considerations

In case additional insulation is required, there exist many RF shielding techniques. This is very important so that harmonic frequencies from the electronics don't cause electromagnetic interference (EMI) and influence the astronomical data. For this reason, a detailed research has been done on the implementation of gaskets within the design. Several factors influence the choice of shielding. The first place to start is at the source. The components emitting the most EMI need to be covered at the source as much as possible. For this reason, the PCB component shielding is the first thing to consider. If the latter cannot be done, there exists several gaskets of all materials and shapes to help with the insulation of small spaces and irregular shapes. In the case of ALBATROS, the observed signal wavelengths are too large to theoretically pass through any gap between the brackets or the metal sheets. Nevertheless, depending on the quality of the manufacturing, additional insulation could be required in the future if more sensitive electronics are added. Depending on the shielding effectiveness wanted, the compression range, the material compatibility, the compression forces and the environmental conditions different solutions apply. The problem also further extends to the frequency of access of the shielded space and the frequencies to be shielded. Below are presented different types of gaskets and their advantages.

Gasket Types	Advantages
Metal RF Gaskets and Spring Contacts	Large compression range Wide frequency range effectiveness Ideal for frequent access
Wire Mesh and Knitted Gaskets	Broad frequency range Good for not frequent access
Oriented Wire	Moisture and rainproof Different types of conductive elastomers
Fabric-Over-Foam	High conductivity and shielding attenuation Low compression forces Large apertures shielding
Electrically Conductive Elastomers	Environmental sealing and EMI shielding High effectiveness at 10 GHz Many materials used
Form-in-Place	Environmental sealing For small and odd shapes Internal and external protection
Board-Level Shielding	Directly soldered to the PCB

Table 3.4: Shielding gaskets comparison [26]



Figure 3.13: Finger stock beryllium copper gasket [11]

Currently, the latest version of the enclosure uses copper tape to insulate at places of small discontinuities. However copper tape is not good for regions which are frequently used. For these cases, finger stock or spring contact gaskets (Figure 3.13) could be added at the junction between two edges if further shielding is needed. In the event that there is a gap at one edge, this solution would restore and improve the shielding effectiveness.

## 3.5 SolidWorks Software

The SolidWorks software is the main software used for the design of the new ALBATROS enclosure. As there is a wide choice of programming languages for heavy computations and algorithm development, the same applies for computer-aided design. Like any essential tool, every software has a certain learning curve. SolidWorks was chosen based on its wide use in the field of astronomy and instrumentation design, for the extensive number of online resources, as well as for its flexible in-built functions. Some of the main features and techniques used are discussed below.

**Creating parts:** Each individual part has a part file before being inserted into the assembly file. The creation of each one starts with a 2D sketch. Geometric relations and dimensions should be given to every line to fully define the sketch.

**Smart Dimensions:** This tool allows the user to either define a fix dimension between two entities or to simply measure resulting dimensions from the assembly. This is one of the most widely used feature within the software.

**Extruded Boss:** This is one of the main features used to go from a 2D sketch to a 3D model. It extends a given plane into a shape with a defined height.

**Extruded Cut:** In the context of the enclosure, this tool was mainly used for the making of the small indentations in the brackets and the shelves. The procedure is to fully define a 2D sketch on an existing part and removing a certain thickness from it. Holes for screws could be made like this, but that is not the most time efficient way of doing so.

**Linear Pattern & Fill Pattern:** These features are used to create a series of holes separated by an equal distance. This was applied for making holes into the brackets and creating the grid for the RF clean space.

**Hole Wizard:** This tool is very convenient for placing holes within the assembly. It has many standard sizes and hole shapes which can be aligned based on the location of other holes. Most of the holes in panels were made through this tool since the panels depend mostly on the size and hole distribution on the brackets.

**Assembly & Mate Parts:** Once each individual part file is created it needs to be assembled by fully defining its geometric relations with respect to the other parts. This needs to be done very carefully because it is easy to over-define parts or accidentally remove parts that are critical to the definition of the rest of the assembly. One important distinction when debugging mating errors is to suppress mating relations instead of deleting them. This way, the relations become inactive instead of being lost.

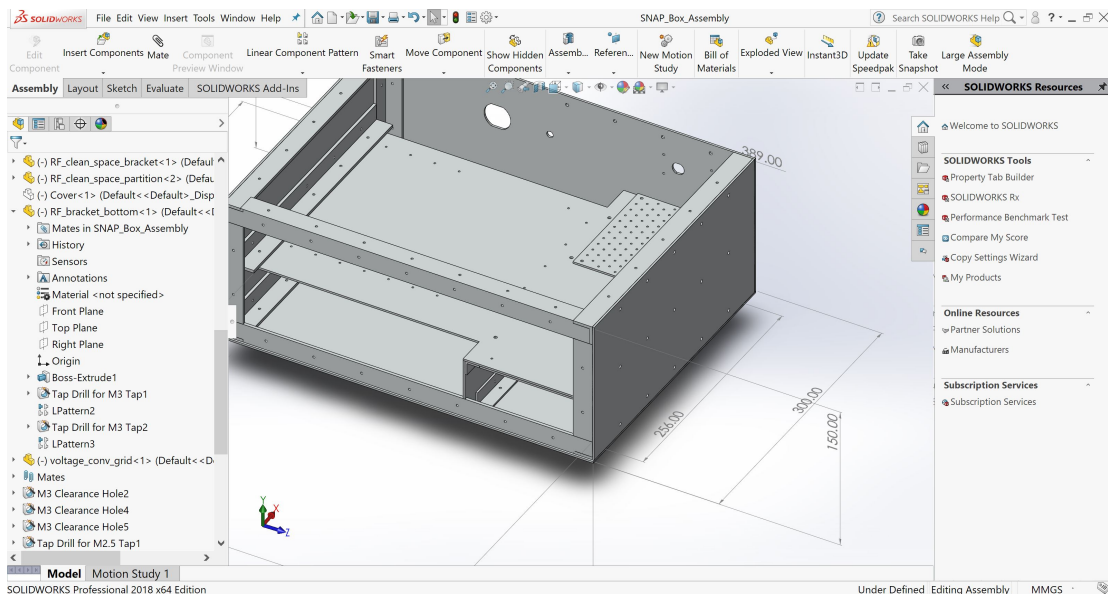


Figure 3.14: SolidWorks assembly screen capture

Figure 3.14 showing the SolidWorks assembly file illustrates how the different tools are accessible through the icons on the top while the active part list and every action and mate defining them is within the drop down menu on the left. Global Hole Wizard actions on the assembly file are shown at the same level as parts since their location is driven by the assembly. For instance, if all the bracket lengths are modified, all the panel holes will follow along. Similarly, every bracket is made using linear patterns, so the average hole separation can be changed through that feature. The hole patterns on the front panels are made into blocks so one could move them around without destroying the hole pattern necessary for a given connector. Fundamentally, there are three kinds of brackets holding the main structure: the vertical bracket, the long horizontal bracket, and the horizontal bracket. For additional flexibility upon modification, the three mated brackets are copied four times within the design such that if their dimensions change, they will change uniformly throughout the enclosure. Note however that the shelf brackets and the RF clean space brackets are slightly different.

Some of the limiting factors to consider when modifying this model is the width of the brackets. Since the indentations in the brackets are used in mating the brackets within the assembly. So if the width is changed, one must also change how the brackets fit in one another. Another important detail is also the sizes of the panels. All mates should be suppressed before changing their sizes, otherwise a lot of errors would appear. Lastly, there are two important holes with defined positions which drive the location of the SNAP board holes and the shelf position. The first hole is located on the middle shelf level on the side panel next to RF clean space, it's the first hole from the back. The second special hole is the one

on the right of the Raspberry Pi connection on the SNAP board located on the same side as the bracket supporting the shelf.

# Chapter 4

## Conclusions

Observing the dark ages is a real technological and environmental challenge. The brightness of the galaxy and the opacity of the ionosphere to lower frequencies has certainly been a limitation since about the 70's. However, today's man-made interference has made it even more difficult to observe the sky in the radio spectrum. From the PRI<sup>Z</sup>M experiment as well as the ALBATROS-EGG first results, it has been shown that the observing conditions on Marion island are ideally suited for low frequency observations given that the RFI there is almost non-existent. The ALBATROS experiment will certainly be a good motivation for moon based low frequency interferometers and similar experiments. Obtaining better experimental data at very high redshift will challenge our current understanding of the early universe, when hydrogen first formed.

Given that the effects of the ionosphere and the galactic noise could be only reduced through calibration or within the data analysis, the remaining variable to take into account during the design of the hardware is to reduce the electromagnetic interference generated by the instrument. This specific element required a thorough design of a new enclosure for the back end electronics. This new version has a fully RF isolated section to shield the signal processing elements before the signal is digitized. Most importantly, this design is very flexible to future changes while fixing issues from previous versions from the ALBATROS-EGG experiment.

Certainly, the design is not straightforward to scale to different dimensions without a proper knowledge of the SolidWorks tools used for the development. In addition, certain holes and dimensions are drivers for the assembly file. Once these limiting components are known, the position of holes can be readjusted and more space can be added if needed. The overall design is meant for the user to be able to open the enclosure from any side and all components to be easily accessible, especially the hard drives which are going to be recuperated for signal correlation post-observation.

This flexible design will certainly not only benefit the ALBATROS project, but could also facilitate this part of the development for the McGill Arctic Research Station where a similar experiment will be deployed. Harsh conditions require precise knowledge of the observing conditions and thus, more house keeping components or more robust hard drives might be required for the next design. The addition of another autonomous station over the period of April-May 2019 on Marion island will provide additional feedback for the back end electronics components and future changes that need to be made.

# Bibliography

- [1] NASA/WMAP science team. Jpl infographics.
- [2] Jim Brau. The interstellar medium gas and dust among the stars, 2016.
- [3] O. Smirnov. *Radio Interferometry: Techniques, Technologies Burning Issues*. Presented at the HRI Techniques - Astronomy Town Meeting, 8 2013.
- [4] Cynthia Chiang. *Intensity Mapping with 21cm Observations*. Presented at the CCA Intensity Mapping Workshop, 2 2019.
- [5] Liju Philip. *The Design, Construction and Deployment of PRIZM*. PhD thesis, University of Kwazulu-Natal, 11 2018.
- [6] CGT Haslam, CJ Salter, H Stoffel, and WEz Wilson. A 408 mhz all-sky continuum survey. ii-the atlas of contour maps. *Astronomy and Astrophysics Supplement Series*, 47:1, 1982.
- [7] Jonathan Pritchard and Abraham Loeb. Cosmology: Hydrogen was not ionized abruptly. *Nature*, 468(7325):772, 2010.
- [8] Cynthia Chiang. *PRI<sup>Z</sup>M:Future Plans*. Presented at the Haystack 21cm workshop, 8 2018.
- [9] Grote Reber. Cosmic static at 144 meters wavelength. *Journal of the Franklin Institute*, 285(1):1–12, 1968.
- [10] Jack Hickish, Zuhra Abdurashidova, Zaki Ali, Kaushal D Buch, Sandeep C Chaudhari, Hong Chen, Matthew Dexter, Rachel Simone Domagalski, John Ford, Griffin Foster, et al. A decade of developing radio-astronomy instrumentation using casper open-source technology. *Journal of Astronomical Instrumentation*, 5(04):1641001, 2016.
- [11] Kemtron. Beryllium copper finger stock.
- [12] George F Smoot. Cmb anisotropies: Their discovery and utilization. *arXiv preprint arXiv:0801.2563*, 2008.
- [13] Chaisson McMillan. *Astronomy Today*. 10. Jim Smith, 1301 Sansome St., San Francisco, 8 edition, 2014.

- [14] David J. Griffiths. *Introduction to Quantum Mechanics*. Pearson, 2 edition, 2005.
- [15] Steven W Ellingson. Sensitivity of antenna arrays for long-wavelength radio astronomy. *IEEE Transactions on Antennas and Propagation*, 59(6):1855–1863, 2011.
- [16] Andrea Isella. *Radio Interferometry: Techniques, Technologies Burning Issues*. Presented at CASA Radio Analysis Workshop, 1 2012.
- [17] Jonathan R Pritchard and Abraham Loeb. 21 cm cosmology in the 21st century. *Reports on Progress in Physics*, 75(8):086901, 2012.
- [18] F De Gasperin, M Mevius, DA Rafferty, HT Intema, and RA Fallows. The effect of the ionosphere on ultra-low-frequency radio-interferometric observations. *Astronomy & Astrophysics*, 615:A179, 2018.
- [19] Jack Singal, J Haider, M Ajello, DR Ballantyne, E Bunn, J Condon, J Dowell, D Fixsen, N Fornengo, B Harms, et al. The radio synchrotron background: Conference summary and report. *Publications of the Astronomical Society of the Pacific*, 130(985):036001, 2018.
- [20] Judd D Bowman, Alan EE Rogers, Raul A Monsalve, Thomas J Mozdzen, and Nivedita Mahesh. An absorption profile centred at 78 megahertz in the sky-averaged spectrum. *Nature*, 555(7694):67, 2018.
- [21] Tankiso H. Moso. *Development of Autonomous Low Frequency Interferometer Stations*. PhD thesis, University of Kwazulu-Natal, 11 2018.
- [22] Steven W Ellingson, Tracy E Clarke, Aaron Cohen, Joseph Craig, Namir E Kassim, Ylva Pihlstrom, Lee J Rickard, and Gregory B Taylor. The long wavelength array. *Proceedings of the IEEE*, 97(8):1421–1430, 2009.
- [23] Trimble Inc. Thunderbolt e gps disciplined clock, 2019.
- [24] R. W. Evans. Design guidelines for shielding effectiveness, current carrying capability, and the enhancement of conductivity of composite materials. Technical Report 1, Tec-Masters Inc., Huntsville, AL United States, 8 1997. Retrieved from NASA Technical Reports Server.
- [25] LearnEMC. Shielding theory.
- [26] EMF Advice. 10 emf shielding materials/fabrics and how to choose one, 2019.